Criteria for extensional necking instability in complex fluids and soft solids.
Part II: imposed tensile stress and force protocols.

D. M. Hoyle* and S. M. Fielding†

Department of Physics, University of Durham, Science Laboratories,
South Road, Durham, DH1 3LE, United Kingdom
(Dated: November 22, 2016)

We study the necking of a filament of complex fluid or soft solid subject to uniaxial tensile stretching, separately under conditions of constant imposed tensile stress and constant imposed tensile force, by means of linear stability analysis and nonlinear simulations at the level of a slender filament approximation. We demonstrate necking to be a flow instability that arises as an unavoidable consequence of the viscoelastic constitutive behaviour of essentially any material (with a possible rare exception). We derive criteria for the onset of necking that can be reported in terms of characteristic signatures in the shapes of the experimentally measured material functions, and that should therefore apply universally to all viscoelastic materials. To confirm their generality, we show them to hold numerically in six constitutive models: the Oldroyd B, Giesekus, non-stretch Rolie-Poly, finite-stretch Rolie-Poly and Pom-pom models, and a simplified toy model of coil-stretch hysteresis, which has a non-monotonic underlying extensional constitutive curve. Under conditions of constant imposed tensile stress, we find two distinct dynamical regimes as a function of the time since the inception of the flow. In the first regime the strain rate quickly attains a value prescribed by the fluid's underlying stationary homogeneous extensional constitutive curve, at the given imposed stress. During this first regime, no appreciable (or only minimal) necking arises. A second regime then ensues in which the initially homogeneous flow destabilises to form a neck. This necking instability can occur via two distinct possible modes. The first mode is relatively gentle and arises in any regime where the slope of the extensional constitutive curve is positive. It has a rate of necking per accumulated strain unit set by the inverse of the slope of the constitutive curve on a log-log plot. The second mode sets in when a carefully defined 'elastic derivative' of the tensile force first slopes down as a function of the time since the inception of the flow. We discuss the way in which these modes of instability manifest themselves in entangled polymeric fluids, demonstrating four distinct regimes of necking behaviour as a function of imposed stress. Under conditions of constant imposed tensile force, typically the flow sweeps up the underlying constitutive curve of the fluid in question, again with instability to necking in any regime where that curve is positively sloping.

I. INTRODUCTION

In developing a constitutive theory for the rheology of a complex fluid or soft solid, key aims are to predict the material's stress response as a function of the applied strain history (or vice versa), in both shear and extension. In comparison with shear, extensional flows typically subject the underlying fluid microstructure (polymer chains, wormlike micelles, *etc.*) to more severe reorganisation. As a consequence, many nonlinear flow features manifest themselves only in extension. In this way, extensional flows prove crucial in discriminating between alternative possible constitutive theories.

To characterise a material's extensional rheology experimentally, a common procedure consists of progressively stretching out in length an initially undeformed cylindrical sample. For a review, see [1]. In stretching at constant imposed Hencky strain rate $\dot{\epsilon}$, the most commonly reported rheological response function is the tensile stress $\sigma_{\mathrm{E}}^+(t)$ as a function of the time t since the inception of the flow. If this can be measured to steady state, the steady tensile stress $\sigma_{\mathrm{E}}^+(t \to \infty)$ plotted as a function of applied strain rate $\dot{\epsilon}$, obtained in a series of filament stretching runs performed at different strain rates, then gives the material's extensional constitutive curve, or flow curve, $\sigma_{\mathrm{E}}(\dot{\epsilon})$. Another common protocol consists of stretching a filament under conditions of a constant imposed tensile stress σ_{E} [2–10]. This typically allows a fluid to attain a stationary flow prescribed by its constitutive curve more readily than stretching at a constant strain rate, making it a preferable protocol for measuring that constitutive curve experimentally [11]. Stretching at constant tensile force F is also commonly performed [12–16].

In these filament stretching procedures, an important aspiration is to ensure that the flow remains as homogeneous as possible, in some part of the sample at least, to allow the measurement of the steady state homogeneous constitutive properties just described. Almost ubiquitously observed during filament stretching, however, is the onset of heterogeneous deformation along the length of the filament. Typically the central region, furthest from the sample ends, develops a higher strain rate than the globally averaged one and thins more quickly than the sample as a whole, hindering attempts to characterise the fluid's homogeneous constitutive properties.

In a typical filament stretching rheometer, the sources of this flow heterogeneity are (at least) twofold. The first is essentially imposed on the fluid externally by the flow geometry, by the no-slip boundary condition that pertains where the fluid makes contact with the rheometer plates. This prevents those parts of the sample that

are nearest the plates from being properly stretched. In consequence, the central regions of the filament, furthest from the plates, thin more quickly than the sample as a whole.

The second source of heterogeneity, in contrast, is intrinsic to the constitutive behaviour of the fluid. It takes the form of a hydrodynamic necking instability, which can be described in simple terms as follows [17, 18]. Consider a filament that is initially stretching in a purely uniform way. Then imagine a local upward fluctuation in strain rate at some location along the filament. Conservation of mass means that the filament must then thin faster in that location. To maintain force balance along the filament a counterbalancing larger stress must then develop in this location. To achieve this larger stress, the fluid must flow faster at that location. This enhances the original fluctuation, giving a positive feedback loop and a runaway instability in which that part of the filament thins more quickly than the filament as a whole, forming a neck.

In practice, of course, these two sources of heterogeneity interact with each other. In particular, the extrinsic geometrical heterogeneity imposed by the no-slip condition at the end-plates provides an initial 'seed' that is then picked up and amplified by the intrinsic hydrodynamic necking instability just described. The necking instability described eventually causes the filament to fail altogether, aborting the experimental run. It has been seen in linear polymers [19], branched polymers [20, 21], associative polymers [22], wormlike micelles [23], bubble rafts [24], and dense colloidal suspensions [25]. It arises in all common stretching protocols, including at constant tensile stress [26], constant tensile force [16], constant imposed Hencky strain rate [21, 27], and following a finite Hencky strain ramp [28].

In a separate manuscript, we studied theoretically the instability to necking of a filament of complex fluid or soft solid subject to stretching under conditions of constant imposed Hencky strain rate [18]. We considered several different constitutive models, with the aim of modelling several different classes of soft material, including: polymer solutions, polymer melts of both linear and branched chain architectures, worm-like micelles and soft glassy materials. Universally across these materials, we found there to be two distinct possible modes of necking instability. The first mode, which has a modest associated growth rate, first becomes unstable in a filament stretching experiment when the extensional stress signal first attains a negative curvature as a function of time since the inception of the flow (or, equivalently, as a function of the accumulated Hencky strain). The second mode, which leads to much more rapid necking, first becomes unstable when a carefully defined 'elastic' derivative of the tensile force with respect to Hencky strain first becomes negative. In the limit of infinite imposed strain rate, we showed that this second mode coincides with the well known Considère criterion for necking in solids [29], which predicts instability when the conventionally de-

fined derivative of the tensile force with respect to Hencky strain first becomes negative. Importantly, however, we also showed that this original Considère criterion fails to correctly predict the onset of necking at finite imposed strain rates.

In this work, we perform the counterpart analysis for filament stretching at a constant imposed tensile stress and (separately) a constant imposed tensile force. (Although this manuscript is intended to be self-contained in its own right, it would most effectively be read alongside its counterpart in [18]. Inevitably, in some places, particularly the introductory sections, the discussion in the present manuscript mirrors that of the controlled strain one.)

Our aims are fourfold. First, we seek to demonstrate that necking is a flow instability that arises as an inevitable consequence of the constitutive behaviour of essentially any complex fluid or soft solid. However we also identify a possible rare exception in which a fluid may be stable against necking, and discuss it carefully.

Second, we shall derive criteria for the onset of necking that are universal to all complex fluids and soft solids, and are reportable simply in terms of characteristic signatures in the shapes of the experimentally measured rheological material response functions. We shall first derive these criteria analytically by means of linear stability calculations performed in a constitutive model of a highly simplified and generalised form. We shall then confirm their generality by performing numerical simulations in six concrete choices of constitutive model: the Oldroyd B, Giesekus [30], non-stretch Rolie-Poly [31], finite-stretch Rolie-Poly [31] and Pom-Pom models [32, 33], and a simplified model of coil-stretch hysteresis [34–36], which has a non-monotonic underlying extensional constitutive curve.

Third, we seek to elucidate the way in which these criteria manifest themselves in entangled polymeric fluids. In particular, in filament stretching experiments performed at constant imposed tensile stress, we predict four distinct regimes of necking as a function of the imposed stress. Fourth, we shall show that the Considère criterion for necking in solids entirely fails to predict necking in complex fluids, and must instead be replaced by the criteria offered here.

Throughout we shall restrict ourselves to the case of a highly a viscoelastic filament of sufficiently large (initial) radius that bulk viscoelastic stresses dominate surface effects in determining the onset of necking. Accordingly, we set the surface tension to zero in our calculations. We therefore do not address capillary breakup as studied in CaBeR rheometers [13, 37–42].

All our calculations assume a slender filament approximation in which the wavelengths of any heterogeneities along the filament's length are long compared to the filament radius. Our calculation therefore cannot capture the final pinch-off of any neck (which would surely in any case be affected by surface tension), nor can it address a more dramatic fracture mode in which the filament

sharply rips across its cross section.

The manuscript is structured as follows. We start in Sec. II with a discussion of our theoretical framework. In particular we introduce the constitutive models and flow geometry under consideration, as well as the slender filament approximation and an exact transformation to the frame that co-extends and co-thins with the filament as it is stretched out. We also outline our linear stability analysis, and the numerical method of our non-linear slender filament simulations. In Secs. III and IV we present results for the protocols of constant imposed tensile stress and constant imposed tensile force respectively. In Sec. V we offer a summary and perspectives for future work.

II.   THEORETICAL FRAMEWORK

A.   Mass balance and force balance

We assume the total stress $\boldsymbol{T}(\boldsymbol{r}, t)$ at time t in a fluid element at position vector $\boldsymbol{r}$ to comprise the sum of a viscoelastic contribution $\boldsymbol{\Sigma}(\boldsymbol{r}, t)$ from the internal fluid microstructure (polymer chains, wormlike micelles, *etc.*), a Newtonian contribution of viscosity η arising from the solvent or other fast degrees of freedom, and an isotropic contribution with a pressure $p(\boldsymbol{r}, t)$:

$$\boldsymbol{T} = \boldsymbol{\Sigma} + 2\eta \boldsymbol{D} - p\boldsymbol{I}. \tag{II.1}$$

The symmetric strain rate tensor $\boldsymbol{D} = \frac{1}{2}(\boldsymbol{K} + \boldsymbol{K}^T)$ where $K_{\alpha\beta} = \partial_\beta v_\alpha$ and $\boldsymbol{v}(\boldsymbol{r}, t)$ is the fluid velocity field. Throughout we shall work in the limit of zero Reynolds number, assuming conditions of creeping flow in which force balance requires:

$$\boldsymbol{\nabla} \cdot \boldsymbol{T} = 0. \tag{II.2}$$

We also assume incompressible flow, with the pressure field $p(\boldsymbol{r}, t)$ determined by enforcing

$$\boldsymbol{\nabla} \cdot \boldsymbol{v} = 0. \tag{II.3}$$

B.   Constitutive models

The dynamics of the viscoelastic stress $\boldsymbol{\Sigma}$ contributed by the internal fluid microstructure (polymer chains, *etc.*) is specified by a constitutive model for the fluid in question. In this work we shall consider several different constitutive models, most of which are fully tensorial and widely used throughout the rheological literature. We also invoke a simplified scalar constitutive model to allow analytical progress in deriving criteria for the onset of necking. We shall then check that the predictions obtained in that model also hold numerically in the tensorial models. We summarise the models now in turn.

1.   Oldroyd B model

The Oldroyd B model provides a phenomenological description of the rheology of dilute polymer solutions. It represents each polymer chain as a dumbbell comprising two beads connected by a Hookean spring. A conformation tensor $\boldsymbol{W} = \langle \boldsymbol{R}\boldsymbol{R} \rangle$ is defined as the ensemble average $\langle \rangle$ of the outer dyad of the dumbbell end-to-end vector $\boldsymbol{R}$, which is taken to have unit length in the absence of flow. The viscoelastic stress is assumed to depend on the conformation tensor according to

$$\boldsymbol{\Sigma} = G\left(\boldsymbol{W} - \boldsymbol{I}\right), \tag{II.4}$$

with a constant modulus G. The dynamics of the conformation tensor obeys

$$\overset{\triangledown}{\mathbf{W}} = -\frac{1}{\tau}\left(\mathbf{W} - \mathbf{I}\right), \tag{II.5}$$

with a characteristic relaxation time τ. The upper convected derivative

$$\overset{\triangledown}{\mathbf{W}} = \frac{D\boldsymbol{W}}{Dt} - \boldsymbol{W} \cdot \mathbf{K} - \mathbf{K}^T \cdot \boldsymbol{W}, \tag{II.6}$$

with a velocity gradient tensor $\mathbf{K}_{\alpha\beta} = \partial_\alpha v_\beta$. This in turn contains the Lagrangian derivative

$$\frac{D\boldsymbol{W}}{Dt} = \frac{\partial \boldsymbol{W}}{\partial t} + \mathbf{v} \cdot \nabla \boldsymbol{W}. \tag{II.7}$$

For an imposed uniaxial extensional flow along the Cartesian $z-$axis we have

$$\boldsymbol{K} = \dot{\epsilon} \begin{pmatrix} -\frac{1}{2} & 0 & 0 \\ 0 & -\frac{1}{2} & 0 \\ 0 & 0 & 1 \end{pmatrix}. \tag{II.8}$$

For any sustained imposed strain rate $\dot{\epsilon} > 1/2\tau$ the Oldroyd B model predicts a dynamical catastrophe in which the dumbbells stretch out indefinitely and the extensional stress diverges. Its extensional constitutive curve, which gives the relationship between the tensile stress $\sigma_{\mathrm{E}} = G(W_{zz} - W_{xx}) + 3\eta\dot{\epsilon}$ and strain rate $\dot{\epsilon}$ in a stationary flow, is therefore undefined for $\dot{\epsilon} > 1/2\tau$. See Fig. 2a).

2.   Giesekus model

The Giesekus model describes more concentrated polymer solutions, by generalising the Oldroyd B model to postulate an anisotropic drag such that the relaxation time of a dumbbell is altered when the surrounding dumbbells are oriented [30]. The dependence of the stress on the conformation tensor remains as in Eqn. II.4, but the conformation tensor now obeys modified dynamics:

$$\overset{\triangledown}{\boldsymbol{W}} = -\frac{1}{\tau}\left(\boldsymbol{W} - \mathbf{I}\right) - \frac{\alpha}{\tau}\left(\boldsymbol{W} - \mathbf{I}\right)^2. \tag{II.9}$$

The parameter α lies in the range $0 \leq \alpha \leq 1$, with Oldroyd B dynamics recovered when $\alpha = 0$. For $\alpha > 0$ the extensional catastrophe of Oldroyd B is averted by the anisotropic drag: the Giesekus model has a well defined constitutive curve at all extension rates. See Fig. 2b).

3.   Rolie-Poly model of entangled linear polymers

As a description of more concentrated solutions or melts of entangled linear polymers, we used the Rolie-Poly model [31]. This starts from microscopic considerations based on the tube theory of polymer dynamics [43], whereby any polymer chain is assumed to be dynamically restricted by a tube of entanglements with nearby chains. If then refreshes its configuration by a process of 1D curvilinear diffusion ("reptation") along the tube contour. Also included are the additional dynamical processes of chain stretch relaxation and convective constraint release [44–46], in which the relaxation of the stretch of any chain acts also to relax entanglement points with other chains, and so facilitate the relaxation of orientation. These processes are modelled via a differential constitutive equation for the the dynamics of the conformation tensor $\boldsymbol{W} = \langle \boldsymbol{RR} \rangle$, with $\boldsymbol{R}$ the end-to-end vector of a polymer chain:

$$\overset{\nabla}{\boldsymbol{W}} = -\frac{1}{\tau_d}\left(\boldsymbol{W} - \mathbf{I}\right) - \frac{2}{\tau_s\left(1 - fT/3\right)}\left(1 - \sqrt{\frac{3}{T}}\right)\left[\boldsymbol{W} + \beta\left(\frac{T}{3}\right)^{\delta}\left(\boldsymbol{W} - \mathbf{I}\right)\right], \qquad \text{(II.10)}$$

where the trace $T = \sum_i W_{ii}$. In this equation, τ_d and τ_s are the characteristic timescales of reptation and chain-stretch relaxation respectively. These are assumed to be in the ratio

$$\frac{\tau_d}{\tau_s} = 3Z, \qquad \text{(II.11)}$$

where Z is the number of entanglements per chain. The parameter β in Eqn. II B 3 sets the degree of convective constraint release, while the factor $(1 - fT/3)$ accounts for finite chain extensibility. (For $f = 0$ the model predicts an Oldroyd B-like stretch catastrophe for a sustained strain rate $\dot{\epsilon} > 1/\tau_s$.)

For a highly entangled sample, with a large entanglement number Z, the chain-stretch relaxes very quickly on the timescale of reptation, $\tau_s \ll \tau_d$. For imposed flow rates $\dot{\epsilon} \ll 1/\tau_s$ we can then take the limit $\tau_s \to 0$ upfront and use the simpler, non-stretching form of the model:

$$\overset{\nabla}{\boldsymbol{W}} = -\frac{1}{\tau_d}(\boldsymbol{W} - \mathbf{I}) - \frac{2}{3}\mathbf{K} : \boldsymbol{W}\left(\boldsymbol{W} + \beta(\boldsymbol{W} - \mathbf{I})\right). \qquad \text{(II.12)}$$

For a value $\beta = 0$ of the convective constraint release parameter, this also recovers the reptation-reaction model of entangled wormlike micelles [47].

4.   Pom-pom model of entangled branched polymers

As a description of the rheology of entangled long-chain branched polymers, we use the Pom-pom model [32, 33]. Each molecule is taken to comprise a linear backbone with an equal number of arms q attached to each end. The relaxation of the arms is assumed to be fast compared to that of the backbone, acting only to provide an additional drag on the backbone dynamics.

The viscoelastic stress is then taken to depend on a conformation tensor $\boldsymbol{W}$ that specifies the orientation of the backbone, and the degree of backbone stretch λ:

$$\boldsymbol{\Sigma} = 3G\lambda^2\left(\mathbf{W} - \frac{1}{3}\mathbf{I}\right). \qquad \text{(II.13)}$$

The dynamics of the backbone orientation is modeled by writing

$$\mathbf{W} = \frac{\mathbf{A}}{\text{tr}(\mathbf{A})}, \qquad \text{(II.14)}$$

with the dynamics of $\mathbf{A}$ then assumed to obey the Maxwell model, Eqn. II.5, with relaxation time τ_b. The backbone stretch has dynamics

$$\frac{D\lambda}{Dt} = \lambda\mathbf{K} : \mathbf{W} - \frac{1}{\tau_s}\left(\lambda - 1\right)e^{\nu^*(\lambda - 1)} \quad \text{for} \quad \lambda \leq q, \quad \text{(II.15)}$$

where $\nu^* = 2/(q - 1)$, subject to an initial condition $\lambda(0) = 1$. A hard upper cutoff is imposed at $\lambda = q$: the extent of backbone stretch is assumed to be entropically bounded by the number of arms attached to each end of the backbone. This hard cutoff leads to catastrophically fast necking in this version of the Pom-pom model, both in the constant imposed Hencky strain rate protocol studied in Ref. [18], and in the constant imposed tensile stress protocol considered below.

The timescales of the backbone orientation and stretch dynamics are assumed to be in the ratio

$$\frac{\tau_b}{\tau_s} = Z_b\phi_b. \qquad \text{(II.16)}$$

Here Z_b is the number of entanglements along the backbone and

$$\phi_b = \frac{Z_b}{Z_b + 2qZ_a}, \qquad \text{(II.17)}$$

which is the fraction of material in the backbone compared with that in the molecule as a whole, with Z_a the number of entanglements along each arm.

Model	Parameters
Oldroyd-B	-
Giesekus	$\alpha = 0.001$
Non-stretch Rolie-Poly	$\beta = 0.0$
Finite-stretch Rolie-Poly	$\beta = 0.0$, $\delta = -0.5$, $\tau_R = 0.00833$ and $f = 0.000625$ $(Z = 40)$
Pom-pom	$\tau_s = 0.1$ and $q = 40$
Hysteresis	$c = 0.001$

TABLE I. Parameter values used in our numerical studies. The solvent viscosity is taken to obey $3\eta = 0.01$ in all models.

5.   Generalised scalar constitutive model

So far, we have outlined the tensorial constitutive models to be studied numerically in the rest of the paper. To allow analytical progress in deriving criteria for the onset of necking we also consider a simplified scalar model [18], which assumes the dominant component of microstructural deformation that develops in a filament stretching experiment to be W_{zz}, where z is the coordinate along the length of the filament. We denote $W_{zz} = Z$ for notational simplicity. (This should not be confused with our use of Z to denote entanglement number in the polymer models above.)

We then consider highly generalised constitutive dynamics for Z, following

$$\frac{DZ}{Dt} = \dot{\epsilon} f(Z) - \frac{1}{\tau} g(Z), \qquad (II.18)$$

with separate loading and relaxation terms characterised by the functions f and g respectively. We intentionally write the model in this highly generalised way, without specifying particular functional forms for the loading and relaxation dynamics $f(Z)$ and $g(Z)$. Our aim in so doing will be to derive criteria for the onset of necking that are reportable simply in terms of characteristic signatures in the shapes of the material's bulk rheological response functions.

The tensile stress then comprises the usual sum of this viscoelastic component and a Newtonian (solvent) contribution:

$$\sigma_{\text{E}} = GZ + \eta\dot{\epsilon}, \qquad (II.19)$$

in which for simplicity, in this scalar model, we have absorbed a factor 3 into the Newtonian viscosity η.

6.   Toy scalar hysteresis model

As a simple model of coil-stretch hysteresis [34–36], which has been observed in polymer solutions, and which is associated with a non-monoonic constitutive curve, we use the scalar model introduced in the previous section, with particular functional choices for f and g:

$$f = 3 + 2Z \qquad (II.20)$$

and

$$g = \frac{Z}{1 + Z^{3/2}} + cZ^2. \qquad (II.21)$$

C.   Units and parameter values.

We use units of length in which the initial length of the filament $L(0) = 1$, and of stress in which the viscoelastic modulus $G = 1$. In any given model, units of time are adopted in which the viscoelastic relaxation timescale is equal to unity. Accordingly for the Oldroyd B and Giesekus models we set $\tau = 1$, the Rolie-Poly model $\tau_d = 1$, and for Pom-pom model $\tau_b = 1$. Values for the other model parameters, in these units, are listed in table I.

D.   Initial conditions, flow geometry and protocol.

We consider a filament that at some initial time $t = 0$ is in the form of an undeformed uniform cylinder of length $L(0)$ in the direction z along the length of the cylinder, and cross sectional area $A(0)$ in the xy plane. The viscoelastic stresses in the material are assumed to be well relaxed in this initial state, such that the molecular conformation tensor $\boldsymbol{W}(0) = \boldsymbol{I}$. At time $t = 0$ the filament is then subject to the switch-on of either a tensile stress or a tensile force, which is held constant thereafter.

As a result of this imposed load, the filament will progressively stretch out in length according to some creep curve in the Hencky strain signal $\bar{\epsilon}(t)$, with the filament length accordingly increasing as $L(t) = L(0)\exp(\bar{\epsilon}(t))$. The overbar signifies that $\bar{\epsilon}$ is the nominal Hencky strain experienced by the sample as a whole: *i.e.*, the Hencky strain averaged along the length of the filament. Once necking arises, the strain and strain rate will locally vary along the filament's length z. For example the Hencky strain rate $\dot{\epsilon} = \dot{\epsilon}(z, t)$, with a $z-$averaged $\dot{\epsilon}$ equal to $\bar{\dot{\epsilon}}$.

E.   Slender filament approximation

We adopt a slender filament approximation [48–50], in which the characteristic wavelengths of any variations in cross sectional area that develop along the filament's

length during necking are taken to be large compared to the filament's radius. This allows us to average the flow variables over the filament's cross section at any location z along it. The relevant dynamical variables are then the cross sectional area $A(z,t)$, the area-averaged fluid velocity in the z direction $V(z,t)$, the extension rate $\dot{\epsilon}(z,t) = \partial_z V$, and any relevant viscoelastic variables contained in the constitutive equations discussed in the previous section.

Within this approximation, the mass balance condition (II.3) is written

$$\partial_t A + V \partial_z A = -\dot{\epsilon} A, \tag{II.22}$$

and the force balance condition (II.2)

$$0 = \partial_z F, \tag{II.23}$$

in which the tensile force

$$F(t) = A(z,t)\sigma_{\mathrm{E}}(z,t), \tag{II.24}$$

and the total tensile stress

$$\sigma_{\mathrm{E}} = G\left(W_{zz} - W_{xx}\right) + 3\eta\dot{\epsilon}. \tag{II.25}$$

The Lagrangian derivative on the left hand side of any constitutive equation is now written:

$$\frac{D}{Dt} = \frac{\partial}{\partial t} + V\frac{\partial}{\partial z}. \tag{II.26}$$

Without sacrificing generality we set the initial cylinder area $A(0) = a_0 = 1$. Although this is in addition to having set the initial cylinder length $L(0) = 1$ (recall Sec. II C above) we emphasize that we are not, in fact, restricting ourselves to scenarios in which the initial area and length are constrained relative to each other in any particular way. Any information about their relative values has simply been lost in making the slender filament approximation.

F.   Transformation to co-extending frame

As the filament stretches out under the imposed tensile stress (or force) its length increases in time as $L(t) = L(0)\exp(\bar{\epsilon}(t))$, and the length-averaged area decreases as $A(t) = A(0)\exp(-\bar{\epsilon}(t))$, where $\bar{\epsilon}(t)$ is the nominal (length-averaged) Hencky strain. To allow for this overall exponential change in the filament's shape as a function of the accumulating strain, it is convenient to make a coordinate transformation to the coextending, cothinning frame by defining new variables of length u, velocity v and area a as follows:

$$\begin{aligned} u &= z\exp(-\bar{\epsilon}(t)),\\ v(u,t) &= V(z,t)\exp(-\bar{\epsilon}(t)),\\ a(u,t) &= A(z,t)\exp(\bar{\epsilon}(t)). \end{aligned} \tag{II.27}$$

The differential operators transform as

$$\partial_z \longrightarrow \exp(-\bar{\epsilon}(t))\partial_u, \tag{II.28}$$
$$\partial_t \longrightarrow \partial_t - \dot{\bar{\epsilon}}u\partial_u. \tag{II.29}$$

We then have transformed equations of mass balance

$$\partial_t a + (v - \dot{\bar{\epsilon}}u)\partial_u a = -(\dot{\epsilon} - \dot{\bar{\epsilon}})a, \tag{II.30}$$

and force balance

$$0 = \partial_u \tilde{F}, \tag{II.31}$$

where the transformed tensile force

$$\tilde{F}(t) = F(t)\exp(\bar{\epsilon}(t)) = a(u,t)\sigma_{\mathrm{E}}(u,t). \tag{II.32}$$

The tensile stress σ_{E} is given as in II.25 above. The Lagrangian derivative on the left hand side of any viscoelastic constitutive equation then becomes

$$\frac{D}{Dt} = \frac{\partial}{\partial t} + (v - \dot{\bar{\epsilon}}u)\frac{\partial}{\partial u}. \tag{II.33}$$

The other (local) terms of the constitutive equations are unaffected by the transformation.

G.   Linear stability analysis

We now discuss our linear stability analysis to determine the onset of necking. This starts by considering a homogeneous "base state" corresponding to a filament that remains a uniform cylinder as it is stretched out, with the flow variables remaining uniform along it. We then add to this base state small amplitude perturbations describing any slight initial heterogeneities along the filament's length, which are the precursor of a neck. (We return below to discuss possible sources for these heterogeneities, in particular in the no-slip condition where the sample meets the rheometer endplates.) Expanding the governing equations to first order in the amplitude of these perturbations then allows us to arrive at a set of linearised equations for the dynamics of the perturbations. Our interest is then in determining whether, and at what time during filament stretching, the perturbations grow into a necked state, or whether they decay to leave a uniform filament.

To allow analytical progress, we shall flesh out the details of the procedure just described in the context of the scalar constitutive model of Sec. II B 5. The entirely analogous (but more cumbersome) calculation for the fully tensorial models is described in detail in Sec. IV of Ref. [18]. It is that calculation which underpins our numerical results in Secs. III and IV below.

Consider first, then, a uniform base state corresponding to a filament that remains a perfect cylinder as it is stretched out, with all flow variables homogeneous along it. In the laboratory frame this obeys the homogeneous

form of Eqns. II.22 to II.25 above, together with the homogeneous form of the scalar constitutive equation. Accordingly the condition of mass balance gives

$$\dot{A}_0(t) = -\dot{\epsilon}_0 A_0. \qquad (II.34)$$

(In the cothinning frame, the base state area a_0 is obviously constant in time by definition.) The tensile force

$$F_0(t) = A_0 \sigma_0, \qquad (II.35)$$

with tensile stress

$$\sigma_0(t) = G Z_0 + \eta \dot{\epsilon}_0. \qquad (II.36)$$

The viscoelastic variable evolves according to

$$\dot{Z}_0(t) = \dot{\epsilon}_0 f(Z_0) - \frac{1}{\tau} g(Z_0). \qquad (II.37)$$

To distinguish this uniform base state from the heterogeneous perturbations to it that we shall go on to consider, we have labelled its flow variables with a subscript 0.

To allow for the possibility of necking, we must now account for spatial variations along the filament's length. Accordingly we return to the spatially aware form of the model equations, expressed for convenience in the co-thinning, co-extending frame: Eqns. II.30 to II.32, together with the scalar constitutive model, Eqn. II.18. We collect these again here for convenience.

The condition of mass balance gives

$$\partial_t a + (v - \bar{\dot{\epsilon}} u) \partial_u a = -(\dot{\epsilon} - \bar{\dot{\epsilon}}) a, \qquad (II.38)$$

while force balance gives

$$0 = \partial_u \tilde{F}, \qquad (II.39)$$

with the transformed tensile force

$$\tilde{F}(t) = F(t) \exp(\bar{\epsilon}(t)) = a(u, t) \sigma_E(u, t). \qquad (II.40)$$

The tensile stress is given by

$$\sigma_E(u, t) = G Z(u, t) + \eta \dot{\epsilon}(u, t), \qquad (II.41)$$

and the viscoelastic variable evolves according to

$$\frac{\partial Z}{\partial t} + (v - \bar{\dot{\epsilon}} u) \frac{\partial Z}{\partial u} = \dot{\epsilon} f(Z) - \frac{1}{\tau} g(Z). \qquad (II.42)$$

We now add to the homogeneous base state small amplitude heterogeneous perturbations, which are the precursor of any neck. For convenience we decompose these into Fourier modes with wavevectors q reciprocal to the space variable u along the transformed filament length:

$$\begin{pmatrix} \dot{\epsilon}(u,t) \\ a(u,t) \\ Z(u,t) \end{pmatrix} = \begin{pmatrix} \bar{\dot{\epsilon}}_0(t) \\ a_0 \\ Z_0(t) \end{pmatrix} + \sum_q \begin{pmatrix} \delta\dot{\epsilon}(t) \\ \delta a(t) \\ \delta Z(t) \end{pmatrix}_q \exp(iqu).$$

$$(II.43)$$

The area perturbations $\delta a(t)$ obey $\delta a(t)/a_0 = \delta A(t)/A_0(t)$ and accordingly measure the fractional variations in cross sectional area along the filament's length, compared to the length-averaged area, at any time t. In this way, they measure the degree of necking.

Expression (II.43) is then substituted into equations (II.38) to (II.42). Expanding in successive powers of the perturbation amplitude, and retaining only terms of first order, then gives a set of linearised equations governing the dynamics of the perturbations.

The linearised mass balance equation is

$$\partial_t \delta a_q = -\delta\dot{\epsilon}_q. \qquad (II.44)$$

The linearised force balance equation is

$$0 = \sigma_E \delta a_q + G \delta Z_q + \eta \delta\dot{\epsilon}_q, \qquad (II.45)$$

and the linearised viscoelastic constitutive dynamics

$$\partial_t \delta Z_q = \delta\dot{\epsilon}_q f(Z_0) + C \delta Z_q. \qquad (II.46)$$

In this equation the term

$$C = \dot{\epsilon} f'(Z_0) - \frac{1}{\tau} g'(Z_0), \qquad (II.47)$$

in which a prime denotes differentiation with respect to a function's own argument.

The strain rate perturbations $\delta\dot{\epsilon}_q$ are instantaneously enslaved to the other variables by the condition of force balance in creeping flow, Eqn. II.45. Accordingly we can eliminate these to arrive at the two-dimensional linear dynamical system:

$$\partial_t \begin{pmatrix} \delta a(t) \\ \delta Z(t) \end{pmatrix}_q = \boldsymbol{M}(t) \cdot \begin{pmatrix} \delta a(t) \\ \delta Z(t) \end{pmatrix}_q, \qquad (II.48)$$

which is governed by the stability matrix

$$\boldsymbol{M}(t) = \begin{pmatrix} \dfrac{\sigma_{E0}}{\eta} & \dfrac{G}{\eta} \\[2ex] \dfrac{-f(Z_0)\sigma_{E0}}{\eta} & -\dfrac{f(Z_0)G}{\eta} + C \end{pmatrix}. \qquad (II.49)$$

We note that this matrix has inherited the (in general) time-dependence of the base state $(\bar{\dot{\epsilon}}_0(t), a_0, Z_0(t))$, upon which it depends.

The stability matrix $\boldsymbol{M}(t)$ does not however depend on the wavevector q, and all Fourier modes $\exp(iqu)$ are predicted to have the same dynamics. We therefore expect the dominant mode in practice to be determined by which is seeded most strongly initially. We return to discuss this issue at the end of Sec. III below.
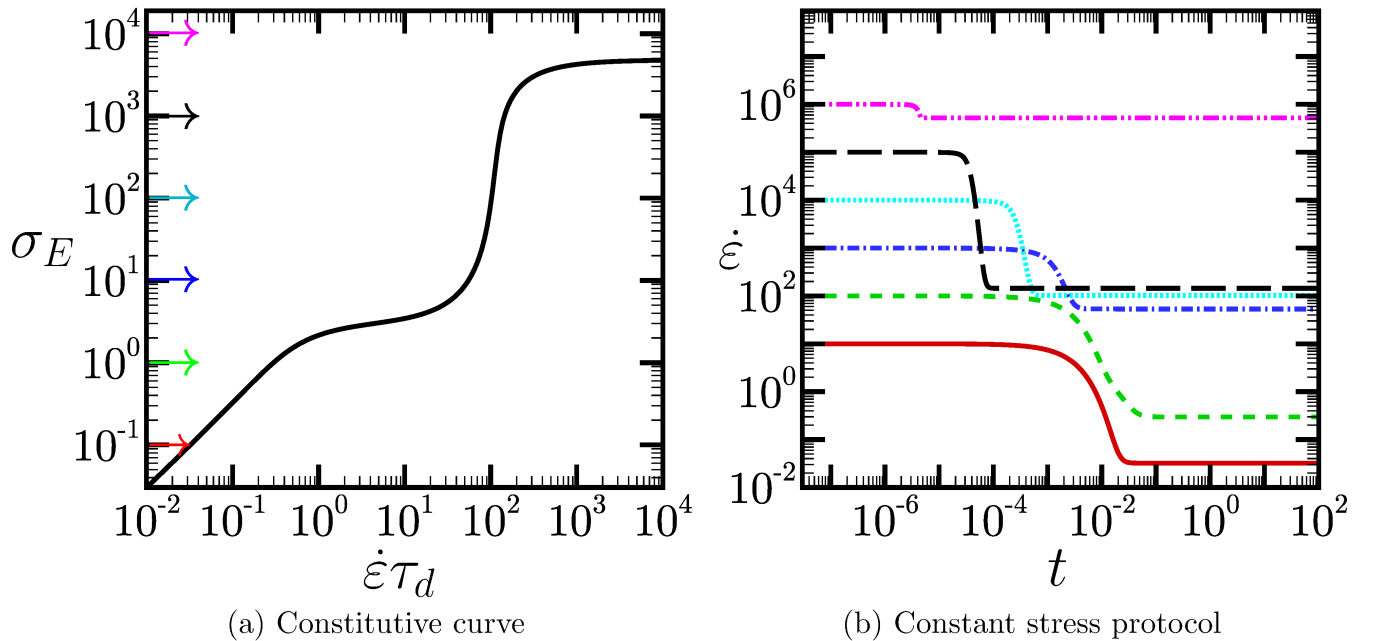
(a) Constitutive curve

(b) Constant stress protocol

FIG. 1. **Finite-stretch Rolie-Poly model: (a) homogeneous stationary constitutive curve for extensional flow, (b) evolution of the strain-rate (of a homogeneous base state flow) to its value prescribed by the constitutive curve, following the switch-on of a constant stress in a previously undeformed sample. Arrows in (a) denote the imposed stress values, each colour-matched to its corresponding transient curve in (b), and with the initial strain rate values in (b) monotonic in the decreasing arrow locations in (a).**

H.   Nonlinear slender filament simulations

To study the dynamics of necking outwith the linear regime, once the amplitude of the necking perturbations is no longer small, we evolve the fully nonlinear slender filament equations II.30 to II.33 numerically. The fact that the length of the filament remains fixed in the co-extending frame in which those equations are expressed, even as the sample stretches out in the laboratory frame, obviates any need for re-meshing the numerical grid over time. Accordingly, we discretize the equations on a fixed mesh and step the equations forward in time by means of an explicit Euler algorithm for the spatially local terms and first order upwinding for the convective ones [51]. Details can be found in Ref. [18], along with a discussion of our approach to ensuring convergence on the space and time-steps, which we also adopt here.

I.   Boundary conditions

In our linear stability calculations we assume periodic boundary conditions between the two ends of the filament (implicitly taking the filament to correspond to a torus being stretched). In our nonlinear slender filament simulations we use an approximate mimic of the no-slip boundary condition between the fluid and the endplates, by adopting an artificially divergent viscosity near each plate according to Eqn. VII.1 of Ref. [18]. As discussed

in that reference, and at the end of Sec. II G above, this automatically provides some heterogeneity that seeds the formation of a neck mid-filament. This in turn is likely to be set by the no-slip condition at the rheometer plates, which constrains the area to remain constant at each plate even as the sample is stretched out overall. The overall effect of this will be to initiate a single neck in the middle of the filament.

III.   CONSTANT STRESS PROTOCOL

In this section we consider a filament of viscoelastic material that is initially cylindrical and undeformed, with all internal stresses well relaxed. It is then subject at some time $t = 0$ to the switch-on of a tensile stress σ_{E0}, which is held constant thereafter. In response to this imposed stress, the most commonly measured bulk rheological signal is the accumulated nominal Hencky strain $\bar{\epsilon}(t)$ as a function of the time t since the stress was applied. This defines the material's extensional creep curve, at the given stress. Sometimes reported instead is its time-differential $\dot{\bar{\epsilon}}(t)$.

Our basic observation in this constant-stress protocol, which our numerical results below will show, is that the sample's response comprises two successive dynamical regimes that are (usually) quite well separated. The first regime is one of fast dynamics at early times after the imposition of the stress, during which the strain rate $\dot{\bar{\epsilon}}(t)$ quickly proceeds to the value prescribed by the material's

stationary homogeneous constitutive curve at the given imposed stress. After this the flow remains steady for the remainder of this first regime. During this first regime, the sample has little or no time in which to develop a neck, and the dynamics can accordingly be motivated by a simple calculation that considers only the homogeneous (base state) dynamics. We outline this in Sec. III A.

After that first fast regime, a second regime then ensues in which the homogeneous flow state destabilises and the sample necks. We shall derive analytical expressions for the rate at which the neck develops in Sec. III B, and give numerical results supporting these in Sec. III C.

A.   Base state: fast evolution to constitutive curve

As just noted, the dynamics at early times after the imposition of the stress can be motivated by a calculation in which the flow is assumed to remain homogeneous, to a good approximation, without necking. (The nominal Hencky strain $\bar{\epsilon}$ therefore corresponds with the true strain ϵ everyone along the filament, so we drop the overbar for the rest of this subsection.) We now sketch the overall features of this early-time response, first analytically in the context of our simplified scalar toy model, then with our numerical results for the full tensorial Rolie-Poly model.

The condition of force balance at constant imposed stress σ_{E} gives

$$\sigma_{\mathrm{E}} = GZ + \eta\dot{\epsilon}. \qquad (\mathrm{III}.1)$$

Within our scalar toy model, the viscoelastic variable Z evolves according to

$$\dot{Z} = \dot{\epsilon}f(Z) - \frac{1}{\tau}g(Z). \qquad (\mathrm{III}.2)$$

Instantaneously after the imposition of the stress the viscoelastic contribution GZ to the stress is zero and the load is all carried by the solvent: a strain rate $\dot{\epsilon} = \sigma_{\mathrm{E0}}/\eta$ therefore immediately develops uniformly along the filament. After this instantaneous initial response, the strain rate then quickly evolves to its value on the constitutive curve at the given stress. This can be motivated by differentiating Eqn. III.1 at constant $\sigma_{\mathrm{E}} = \sigma_{\mathrm{E0}}$ to get

$$\begin{aligned}\dot{\bar{\epsilon}} &= -\frac{G}{\eta}\dot{Z} \\ &= -\frac{G}{\eta}\left[\dot{\epsilon}f(Z) - \frac{1}{\tau}g(Z)\right], \qquad (\mathrm{III}.3)\end{aligned}$$

where we have substituted $\dot{Z}$ from Eqn. III.2 in moving from the first to the second line. In the second line, the argument Z of f and g is given by $Z = \frac{1}{G}(\sigma_{\mathrm{E}} - \eta\dot{\epsilon})$ with constant $\sigma_{\mathrm{E}} = \sigma_{\mathrm{E0}}$. In this way, Eqn. III.3 prescribes the evolution of the strain rate $\dot{\epsilon}$ on a fast timescale η/G to its value on the stationary homogeneous constitutive curve at the given imposed stress σ_{E0}.

We have motivated this early-time evolution here in the context of our simple scalar model. However the same scenario arises in the full tensorial constitutive models used throughout the rest of the paper. Numerical results for the (homogeneous flow response of the) fully tensorial Rolie-Poly model are shown as an example in Fig. 1b). For each imposed stress value, the instantaneous appearance of a strain rate $\dot{\epsilon} = \sigma_{\mathrm{E0}}/\eta$ at time $t = 0$ is clear, followed by fast evolution over a time interval that scales as the short timescale η/G to the strain rate prescribed by the corresponding constitutive curve in Fig. 1a), for the given imposed stress.

B.   Linear instability: rate of necking

Following the fast evolution to a homogeneous flow state prescribed by the stationary constitutive curve, as just described, a second dynamical regime ensues in which that homogeneous flow state destabilises and the sample starts to neck. We now perform a linear stability analysis to determine the dynamics of the onset of this necking process. To allow analytical progress, we do this within our simplified scalar model. We intentionally leave the form of the loading and relaxation functions $f(Z)$ and $g(Z)$ unspecified. Our aim in so doing is to motivate formulae for the rate of necking that can be expressed in terms of characteristic features in the shape of the underlying homogeneous constitutive curve, independently of any specific constitutive choices for f and g (or their counterparts in any fully tensorial model).

With the possibility of heterogeneous flow reinstated, the flow is now governed by Eqns. II.38 to II.42. Within these equations we consider a uniform time-independent base flow state $\dot{\epsilon}_0, a_0, Z_0$, as pertaining at the end of the early-time regime described in Sec. III A, with the strain rate $\dot{\epsilon}_0$ prescribed by the underlying homogeneous constitutive for the given imposed stress. To this initially homogeneous state we then add small amplitude heterogeneous perturbations, as set out in Eqn. II.43, which are the precursor of a developing neck. (Note that, although for the sake of pedagogy in this analytical section we describe the development of heterogeneity as starting only after the early fast evolution of Sec. III A above, in practice these two regimes are only separated to good approximation. To account for any slight mixing of the two regimes, our numerics in Sec. III C allow for heterogeneity right from the inception of the flow.)

Substituting Eqn. II.43 into Eqns. II.38 to II.42, expanding in powers of the amplitude of the perturbations, and discarding any terms higher than those of first order, gives the set of linearised equations II.44 to II.47, which govern the time evolution of the perturbations. These can finally be expressed in matrix format as in Eqns. II.48 and II.49. Because the base state variables upon which the stability matrix $\boldsymbol{M}$ depends have already attained stationary values on the underlying constitutive curve by the end of the first fast regime, the matrix $\boldsymbol{M}$

that we need to consider for this protocol is in fact time-independent. Instability to necking will obtain in any regime where M has at least one eigenvalue that is positive, in the sense of having positive real part, with the associated rate of necking being governing by the amplitude of that real part. Our aim now, therefore, is to understand when any eigenvalue of M is positive, and the way in which the rate of necking that it prescribes relates to any quantities that could be measured experimentally.

The two eigenvalues of M follow as solutions of

$$\omega^2 - T\omega + \Delta = 0, \tag{III.4}$$

where T is the trace of M and Δ its determinant.

The trace T of M is given by

$$T = \frac{1}{\eta}(\sigma_{E0} - fG) = -\frac{1}{A(0)\eta}\partial_\epsilon F_{\text{elastic}}. \tag{III.5}$$

(We shall return below to explain the meaning of the derivative $\partial_\epsilon F_{\text{elastic}}$ in this expression.) The determinant Δ of M is given by

$$\Delta = \frac{\sigma_{E0}C}{\eta} = -\frac{f}{\eta}\left[\frac{d\log\sigma_{E0}}{d\dot\epsilon}\right]^{-1}. \tag{III.6}$$

(Note that the solvent viscosity η is small compared to the viscoelastic viscosities, and we have ignored terms $O(1)$ compared to those $O(G/\eta)$ in these expressions.) In each of Eqns. III.5 and III.6, the second equality follows from the first by a few lines of algebra, which we do not write down.

The first mode of necking instability arises in any regime where the determinant $\Delta < 0$, with a rate of necking per unit time that scales as the inverse logarithmic derivative of the material's underlying homogeneous constitutive curve:

$$\omega \sim \left[\frac{d\log\sigma_{E0}}{d\dot\epsilon}\right]^{-1} \quad \text{``Constitutive curve mode''}. \tag{III.7}$$

This is a key result. It predicts that any material with a positively sloping homogeneous extensional constitutive curve will be unstable to necking [17, 18]. Because the vast majority of complex fluids and soft solids have such a curve, we predict that essentially all materials will neck when subject to extensional stretching. This prediction is indeed consistent with ubiquitous reports of necking in the experimental literature.

The result in (III.7) also tells us that a material will neck relatively more quickly in any regime in which its homogeneous constitutive curve of stress as a function of strain rate is relatively flatter. This is intuitively understood as follows. Consider an initially homogeneous filament. Then suppose that the strain rate fluctuates upward slightly (compared to the averaged imposed one) in some local region of the filament. As a result of this, the filament will thin a bit faster in that locality compared to the filament as a whole. In order to maintain a uniform force along the length of the filament, as required by the force balance condition, a counterbalancing stress must be provided in the developing neck to compensate for the thinned area. To generate this, an even faster flow must develop in that slightly necked region. This enhances the original fluctuation, giving positive feedback and instability to necking. The extent to which the material must indeed flow faster to provide a counterbalancing stress in the developing neck is determined by the inverse slope of its constitutive curve at the relevant imposed stress, which therefore controls the rate of necking according to Eqn. III.7.

In additional to the "constitutive-curve" mode just discussed, a second mode predicts necking in any regime where the matrix M has trace $T > 0$, and so where

$$\partial_\epsilon F_{\text{elastic}} < 0 \quad \text{``Elastic Considère mode''.} \tag{III.8}$$

The associated eigenvalue, which determines the rate of necking per unit time associated with this mode, is $O(G/\eta)$, which is large for the highly viscoelastic materials considered here. This second mode was also predicted in Ref. [18] as a route to necking in the protocol of imposed Hencky strain rate. As discussed in Ref. [18], the derivative $\partial_\epsilon F_{\text{elastic}}$ of the base state's tensile force with respect to strain ϵ needs careful explanation. It is defined by evolving the system's state up to some strain ϵ with the full model dynamics, including loading by flow as encoded by f and relaxation as encoded by g. In the next increment of strain $\epsilon \to \epsilon + \delta\epsilon$ over which the derivative is taken the relaxation term $g(Z)$ is then suppressed, with only the elastic loading dynamics implemented.

Whether any means can be found of measuring this derivative experimentally is an open question, which we do not address here. However we do emphasise that the condition $\partial_\epsilon F_{\text{elastic}} < 0$ just discussed is *not* the same as the condition $\partial_\epsilon F < 0$. The "elastic" Considère criterion proposed here is therefore *not* the same as the original Considère criterion for necking. Indeed, in any experiment performed at constant tensile stress σ_{E0} the force $F = A\sigma_{E0}$ decreases with increasing strain for all times after the imposition of the load, because the stress is constant (by definition) and the filament's area always thins with strain as $A \sim \exp(-\bar\epsilon(t))$. Therefore, the original Considère criterion entirely fails to predict necking in a constant stress protocol: it must be replaced by the two new criteria offered here.

C.   Numerical results

1.   Linear regime

In the previous subsection we derived criteria for two different modes of necking instability under conditions of constant imposed tensile stress. To allow analytical progress, we did this in the context of our simplified and highly generalised scalar constitutive model. In

this section, we shall present numerical results confirming the validity of these criteria in six concrete choices of constitutive model, and discuss in more detail the way in which the two modes of necking manifest themselves in the various flow regimes of these models. The first five models (Oldroyd B, Giesekus, non-stretch Rolie-Poly, finite-stretch Rolie-Poly and Pom-Pom) are fully tensorial and popularly studied in the rheological literature. The sixth is a toy model of coil-stretch hysteresis, which we constructed so as to have a non-monotonic constitutive curve, in order to demonstrate stability against necking in the regime of negative constitutive slope $\sigma_{\mathrm{E}}'(\dot{\epsilon}) < 0$.

We start in Fig. 2 by showing the underlying homogeneous constitutive curve for each of the six models. As discussed above, following the imposition of a constant stress $\sigma_{\mathrm{E}0}$, the strain rate first evolves rapidly to its value as prescribed by this underlying constitutive curve, with the sample remaining (almost) uniform while that happens. The constitutive curve mode discussed above then predicts instability to necking in any regime where that curve has positive slope. (As we shall find below, the elastic Considère mode will also arise in two of the models studied, although in relatively restricted regimes of flow rate.) Its onset rate per unit time is given by Eqn. III.7. Correspondingly, its onset rate per unit strain is given by

$$\frac{\omega}{\dot{\epsilon}} \sim \left[\frac{d\log\sigma_{\mathrm{E}0}}{d\log\dot{\epsilon}}\right]^{-1} \quad \textbf{``Constitutive curve mode''},$$

(III.9)

that is, by the inverse of the derivative of the constitutive curve as shown in a log-log representation.

This rate is indicated by the colourscale in each of the constitutive curves in Fig. 2: faster necking (as a function of accumulated strain) is seen in regimes of flatter positive constitutive slope. In the regime of negative constitutive slope of the hysteresis model (panel f), stability against necking is predicted.

With these general remarks in mind, we now explore in detail the necking dynamics of these six models under conditions of constant imposed tensile stress. Each panel (a)-(f) of Fig. 3 corresponds to its counterpart constitutive curve panel in Fig. 2, and comprises two separate subgraphs. The lower subgraph in each case essentially reproduces the corresponding constitutive curve of Fig. 2, but with the axes inverted so as to have the stress on the abscissa, as the imposed quantity in this protocol. At any imposed stress, the expected rate of necking as a function of accumulated strain is again shown by the colourscale according to Eqn. III.9.

The upper subgraph in each panel of Fig. 3 shows the necking dynamics in detail. The data are presented in the plane $(\bar{\epsilon}, \sigma_{\mathrm{E}})$ of accumulated strain and imposed stress, and should be interpreted as follows. Any vertical cut up this plane corresponds to single experiment in which the imposed tensile stress σ_{E} is held fixed and the accumulated strain $\bar{\epsilon}$ increases up the plane as the filament stretches out under the influence of this applied load. At any imposed stress value σ_{E}, the magenta dashed line

shows the strain at which the strain rate attains its value on the stationary underlying constitutive curve, to within 1%, following the fast early-time dynamics described in Sec. III A.

The solid black lines show contours of constant area perturbation $\delta a(t)$, with each successive contour crossing corresponding to an increase by a factor $10^{1/4}$ in the degree of necking $\delta a(t)$. The nth contour thus represents a degree of necking $\delta a/\delta a_0 = 10^{n/4}$, where δa_0 is the small initial seeding at the start of the run. The more densely clustered the contour lines vertically at any fixed σ_{E}, therefore, the faster necking occurs in an experiment at that imposed stress. In each panel of Fig. 3 we have shown only the first 20 contour lines, assuming that the sample will have failed altogether by this time. An indication of the dependence of the strain at which the sample will finally fail on the imposed stress is given by focusing on one representative contour.

Consistent with the claim made in Sec. III A above, only a small amount of necking occurs (few contour lines are crossed) during the fast early-time regime in which the strain rate rapidly evolves to the stationary underlying constitutive curve. Beyond that early regime, the neck indeed develops (contour lines are crossed) at a rate consistent with the scaling prediction of (III.9), set by the inverse of the slope of the underlying constitutive curve in its log-log representation. We now discuss in more detail the way this basic observation manifests itself in the different flow regimes of each model.

In the Oldroyd B model, the constitutive curve has a constant initial slope $\sigma_{\mathrm{E}}'(\dot{\epsilon}) = 3$ in the Newtonian regime at low strain rates. See Fig. 2a. The associated rate of necking per unit strain is likewise modest and constant as a function of strain rate, as seen in Fig. 3a). For higher imposed stresses the constitutive curve is a much steeper function of strain rate, due to the well-known extensional catastrophe of this model, which we recall predicts a divergent stress for strain rates $\dot{\epsilon} > 1/2\tau$. This greatly stabilises the filament against necking, as seen by the near vertical contour lines in Fig. 3a for larger imposed stresses.

In the Giesekus model the divergent constitutive curve of the Oldroyd B model is avoided and the stress remains finite at all strain rates. Nonetheless, a vestige of the Oldroyd B catastrophe is seen in the steeply sloping section at strain rates $\dot{\epsilon} \approx 1/2$ in Fig. 2b. Accordingly, the model predicts a regime of relatively slow necking for imposed stresses $10^1 < \sigma_{\mathrm{E}} < 10^3$ in that regime of steep constitutive slope, and so of relatively flat strain rate versus stress. This is indeed seen in that stress range $10^1 < \sigma_{\mathrm{E}} < 10^3$ in the contour map of Fig. 3b). Faster necking is seen for imposed stresses on either side of this window, where the constitutive curve of Fig. 2b is Newtonian at low flow rates, or quasi-Newtonian at high flow rates.

The constitutive curve of the non-stretch Rolie-Poly model (Fig. 2c) has a Newtonian regime at low strain rates, in which chain orientation progressively increases
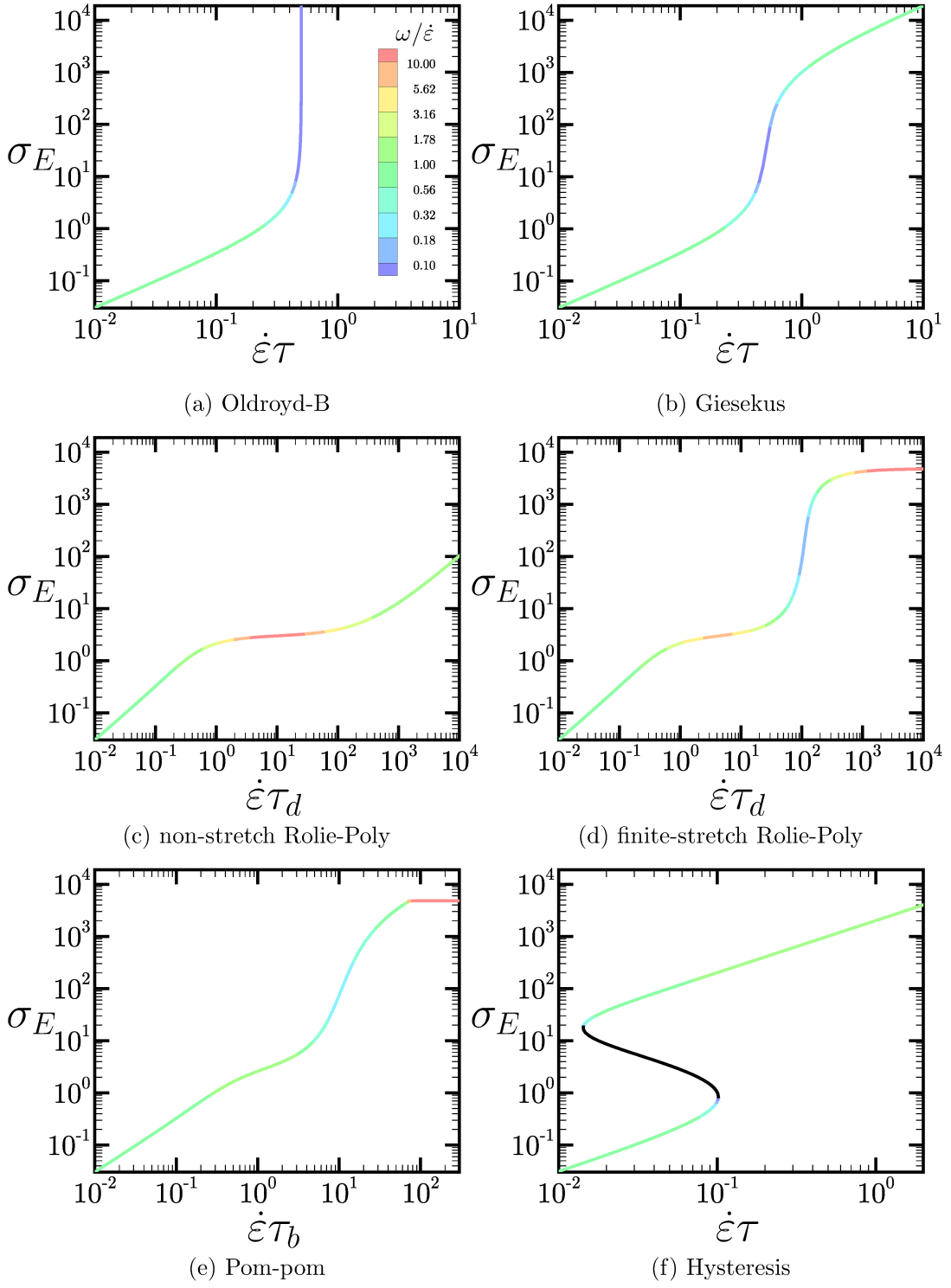
FIG. 2. **Constitutive curves of the models to be studied. The colourscale in each case shows the value of** $[d \log \sigma_{\mathrm{E}} / d \log \dot{\epsilon}]^{-1}$**, which sets the rate of necking per unit strain according to Eq. III.9. Any regime in which this quantity is less then or equal to zero, indicating stability against necking, is shown in black.**

with increasing applied strain rate. Once the strain rate $\dot{\epsilon} = O(1/\tau_d)$, however, the orientation saturates and the stress becomes a much flatter function of strain rate, rising again only at much higher strain rates when the sol-

vent contribution $3\eta\dot{\epsilon}$ becomes important. For imposed stresses $\sigma_{\mathrm{E}} \approx 3.0$ corresponding to the flat region where $\dot{\epsilon} = O(1/\tau_d)$, therefore, we expect very rapid necking via the constitutive curve mode. This is confirmed in
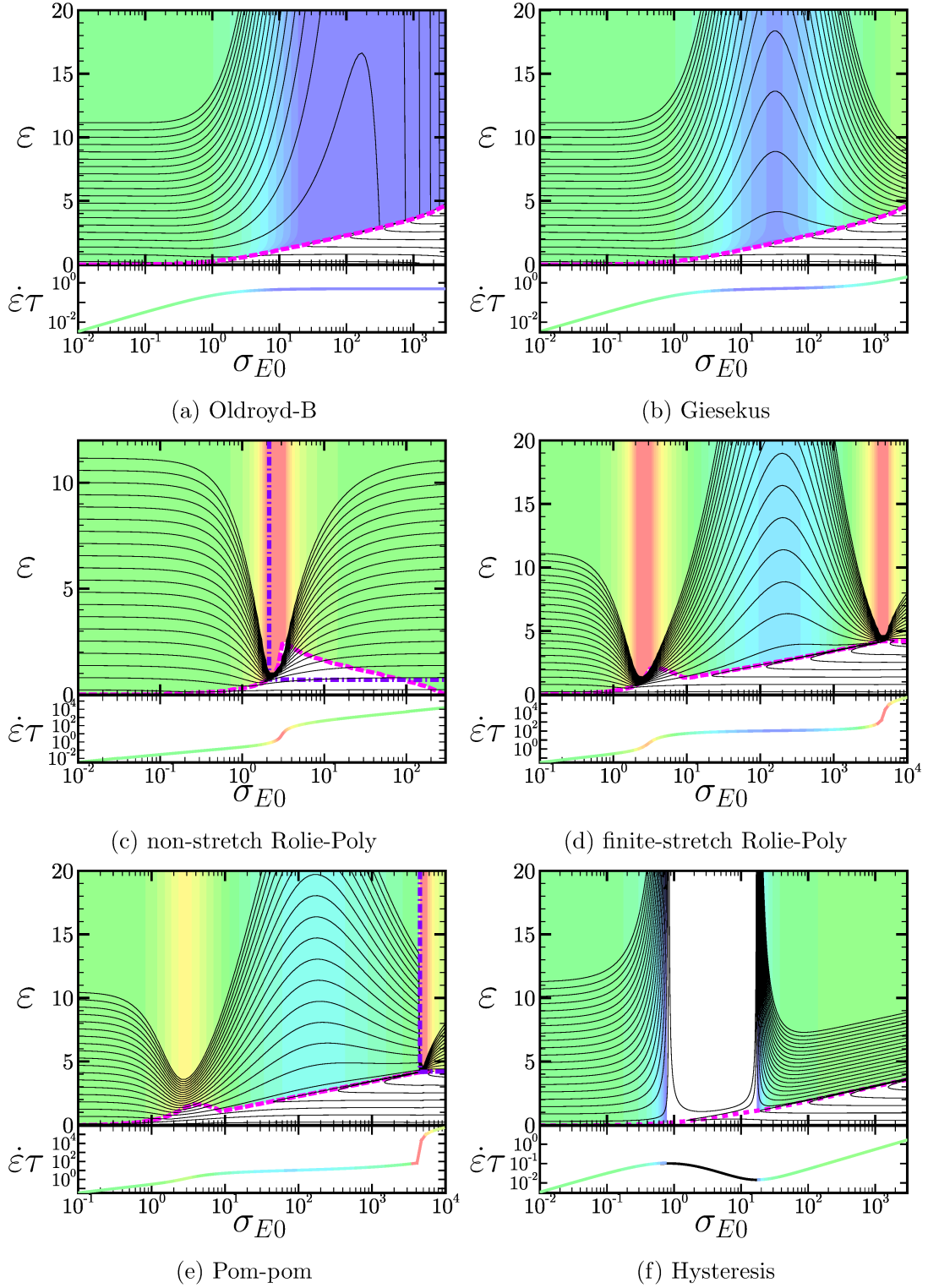
(a) Oldroyd-B

(b) Giesekus

(c) non-stretch Rolie-Poly

(d) finite-stretch Rolie-Poly

(e) Pom-pom

(f) Hysteresis

FIG. 3. **Numerical results for the linearised necking dynamics at constant imposed tensile stress within the six constitutive models. In each panel the lower subfigure shows the inverted constitutive curve, with the rate of necking (per unit strain) according to the constitutive curve mode shown on the same colourscale as in Fig. 2. The upper subfigure in each panel explores the necking dynamics in more detail. Here the thin black lines show contours of constant area perturbations $\delta a / \delta a_0 = 10^{n/4}$, with $n = 1 \cdots 20$ in curves from bottom to top, representing the growing degree of necking at increasing strain ϵ upwards in any filament stretching experiment at fixed imposed stress σ_{E0}. The magenta dashed lines show the strain at which the underlying base state attains a state of stationary flow on the underlying homogeneous constitutive curve, to within 1%. The purple dot-dashed line shows the strain at which the elastic Considère mode becomes unstable. The colours denote the rate of necking, with the same colourscale as in 2. Regions of stability against necking are shown in white.**

Fig. 3c).

In fact for imposed stresses $\sigma_E \gtrsim 2.0$ the elastic Considère mode is also active, as indicated by the purple dot-dashed line. According to Eqn. III.8, this predicts a rate of necking $O(G/\eta)$ per unit time, which is very fast. (Recall that the solvent viscosity η is small compared to the zero shear viscosity of the viscoelastic components.) However it is important to note that the corresponding rate of necking per unit strain is $O(G/\eta\dot{\epsilon})$. Now the constitutive curve of this model, in this regime where chain orientation has saturated, is dominated by the solvent contribution. Accordingly the associated strain rate $\dot{\epsilon} = \sigma_E/\eta$. Combining these gives a rate of necking $O(G/\sigma_E) = O(1)$ per unit strain, which remains relatively gentle. This is indeed confirmed by our numerical results to the right of Fig. 3c): because both the rate of necking and the rate of straining are fast, $O(G/\eta)$, the rate of necking per unit strain remains $O(1)$.

The Rolie-Poly model with chain-stretch now included is explored in Figs. 2d) and 3d). For strain rates $\dot{\epsilon} < 1/\tau_R$, its dynamics essentially match that of its non-stretch counterpart discussed in the previous paragraph, consistent with the fact that negligible chain stretch develops for imposed flow rates lower than the rate of chain stretch relaxation. Once the strain rate $\dot{\epsilon} = O(1/\tau_R)$, however, significant chain stretch develops and the constitutive curve stress rises rapidly as a function of strain rate. For imposed stresses corresponding to this regime, much slower necking is predicted: note the blue colourscale in Fig. 2c). This is indeed observed, via the widely spaced contour lines for imposed stresses in the range $10^1 - 10^3$ in Fig. 3d). At higher stresses still the chain stretch saturates, the constitutive curve is much flatter, and the necking is much faster.

The dynamics of the finite-stretch Rolie-Poly model can therefore be categorised into four distinct regimes, as follows. For low imposed stresses, corresponding to strain rates in the regime $\dot{\epsilon} < 1/\tau_d$ in Fig. 2d), the model shows essentially Newtonian response: the constitutive curve has a constant slope $\sigma'_E(\dot{\epsilon}) = 3$, and the rate of necking is likewise modest and independent of stress. For imposed stresses $\sigma_E \approx 3.0$ the chain orientation has saturated and the constitutive curve is a relatively flat function of strain rate, giving very fast necking. For imposed stresses in the range $10^1 - 10^3$ the constitutive curve has large slope due to the development of chain stretch in that regime, and the rate of necking is accordingly much lower. Finally at high stresses the chain stretch saturates, the constitutive curve is much flatter, and necking occurs very quickly. We note that the elastic Considère mode, which was present in the non-stretch Rolie-Poly model, is absent in the stretching version of the model.

The Pom-Pom model is explored in Figs. 2e) and 3e). Comparing Figs. 2d) and 2e), we see that the constitutive curve of the Pom-Pom model also shows four regimes, which resemble those of the finite-stretch Rolie-Poly model. Indeed in close analogy with the dynamics of the Rolie-Poly model, these regimes are associated with

a progressive increase then saturation in backbone orientation, for strain rates $\dot{\epsilon} = O(1/\tau_b)$ and their counterpart imposed stresses, followed by an increase then saturation in backbone stretch, for strain rates $\dot{\epsilon} = O(1/\tau_s)$ and their counterpart imposed stresses.

The Pom-Pom model accordingly shows very similar necking dynamics to those of the Rolie-Poly model, as can be seen by comparing Figs. 3d) and 3e). However at the highest imposed stresses there is an importance difference between the two models: in the Pom-Pom model the backbone stretch is assumed to have an infinitely sharp cutoff, compared with the more gentle saturation in the chain stretch of the Rolie-Poly model. This gives an essentially flat regime in the constitutive curve at the right hand side of Fig. 2e), which manifests itself in Fig. 3e) as very violent necking via the elastic Considère mode. Whether this cutoff is physically realistic remains an open question, which we discussed in the context of necking under conditions of constant imposed Hencky strain rate in Ref. [18].

Finally in Fig. 3f) we explore the necking dynamics of our toy model of coil-stretch hysteresis, for which the underlying constitutive curve is non-monotonic (Fig. 2f). The important point to note here is that filament is stable against necking for imposed stresses in the regime of negative slope in that constitutive curve. Whether a different mode of extensional failure would take over in practice remains an open question.

2.   Nonlinear dynamics

So far we have discussed necking dynamics in the linear regime, in which the amplitude of the growing necking perturbations still remains small. To study the necking dynamics outwith the linear regime, once the amplitude of the heterogeneous perturbations becomes non-negligible, we simulated the full nonlinear slender filament equations.

Results for the finite-stretch Rolie-Poly model are shown in Fig. 4. Panel a) shows the equivalent, for these nonlinear calculations, of the linear stability results discussed above in Fig. 3d). As usual, a vertical cut up this plane of strain ϵ and stress σ_{E0} represents a single experiment performed at a given imposed tensile stress σ_{E0}. The experiment starts with an initially unstretched filament at $\epsilon = 0$, then the accumulated strain ϵ increases up the plot as the filament progressively stretches out.

The thin black lines then show contours of constant $\Lambda(t) \equiv A_{\text{hom}}(t)/A_{\text{mid}}(t)$, where $A_{\text{hom}}(t)$ is the filament area calculated at any time t by supposing the filament were stretching in a purely uniform way, and $A_{\text{mid}}(t)$ is the actual cross sectional area at the filament's midpoint. In this way, $\Lambda = 1$ corresponds to a uniform filament, and Λ progressively increases as the filament necks. The first contour has $\Lambda = 1$, and each successive contour as ϵ increases at fixed σ_{E0} indicates an increase in Λ by a factor $4^{1/20}$. The 20th contour, which is the final shown,
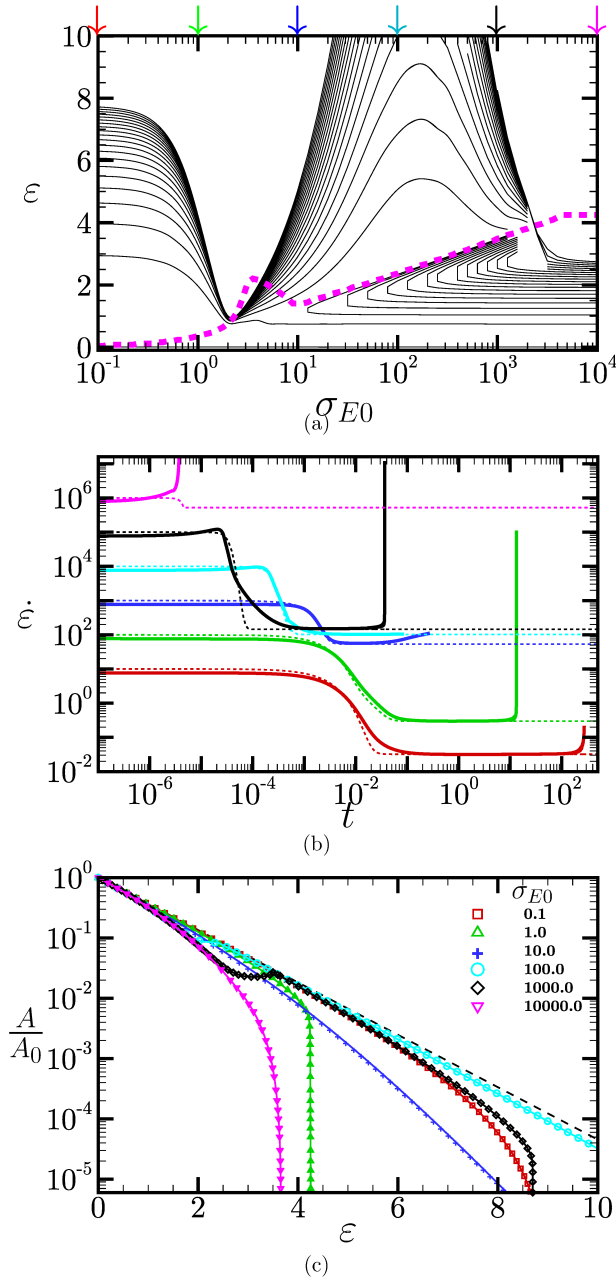
(a)

(b)

(c)

FIG. 4. **Necking dynamics in nonlinear slender fila-
ment simulations of the Rolie-Poly model of linear
entangled polymers under conditions of constant im-
posed tensile stress. (a) Thin black lines show con-
tours of constant of necking heterogeneity, Λ, with the
n^{th} contour having $\Lambda = 4^{n/20}$. Also shown by the ma-
genta dashed line is the strain at which the sample
attains a state of flow on the homogeneous consti-
tutive curve to within 1%, which occurs before sig-
nificant necking develops. The sharp corners in some
earlier contours are an artefact of a breakdown in our
interpolation. For the six imposed strain rates indi-
cated by arrows in (a), the evolution of the nominal
strain rate as a function of time since the inception
of the flow is reported in (b) for both the nonlin-
ear simulation (solid lines) and for a calculation in
which the filament is artificially assumed to remain
uniform (dashed lines). Counterpart results for the
filament's cross sectional area are shown in (c): as-
suming homogeneous flow (dashed black line) and at
the filament's midpoint in a calculation that allows
for necking (symbols and solid lines).**

therefore represents $\Lambda = 4$. (Although this ratio of ar-
eas is relatively modest we note that the sample is close
to necking by this time, because the global area has be-
come very small.) Accordingly we show only the first 20
contour lines, and simply assume that the sample will
fail altogether by some final pinch-off event before this
contour is attained. We note, however, that our slen-
der filament calculation is not capable of capturing the
dynamics of the final pinchoff, because it assumes varia-
tions along the filament to be gentle on the scale of the
filament radius. It also neglects any physics on the mi-
croscopic lengthscales associated with the surface tension
of the interface, which would surely affect the final stages
of failure.

Comparing Fig. 4a) with Fig. 3d), we see that our sim-
plified linear calculation in fact already performed rather
well in predicting the onset of necking in the full non-
linear calculations. Any differences in the quantitative
detail between the two plots can be explained by the fact
that the material functions at the filament's midpoint in
the nonlinear simulations differ slightly from those in the
base state of the linear calculation.

The necking dynamics at the six imposed stress values
denoted by arrows in Fig. 4a) are presented in further
detail in panels b) and c). Panel b) shows the evolution
of the nominal (length-averaged) strain rate as a function
of time since the inception of the flow for the nonlinear
simulation (solid lines), and the strain rate predicted by a
calculation in which the filament is artificially assumed to
remain uniform (dashed lines). In each case except that
of the highest imposed stress, the strain rate attains its
value prescribed by the homogeneous constitutive curve
with only minimal necking occurring transiently en route
to that curve. A second flow regime then ensues in which
this state of homogeneous flow on the constitutive curve
destabilises and the strain rate increases as the filament
necks. Counterpart results for the cross sectional area at
the filament's midpoint are shown in (c). This follows
the exponential prediction of the homogeneous calcula-
tion until necking occurs, when the signal plunges below
the homogeneous predictions. The least necking arises for
the imposed stress value $\sigma_{E0} = 100.0$, which corresponds
in the constitutive curve Fig. 2d) to a strain rate of or-
der $1/\tau_R$, in the regime where chain stretch is rapidly
developing with increasing strain rate. Indeed, at this
stress value the flow remains on the underlying constitu-
tive curve without any appreciable necking effects up to
the final strain $\epsilon = 10.0$ considered. The most dramatic
necking in Fig. 4c) arises for an imposed stress $\sigma_{E0} = 1.0$,
in the regime of saturated orientation in the constitutive
curve of Fig. 2d). Fig. 4(b) demonstrates that for larger
imposed tensile stresses there is a smaller time-window
over which the strain rate accords with its value as pre-
dicted by the stationary homogeneous constitutive curve,
before necking causes it to deviate significantly. This has
been observed experimentally: see, for example, Fig. 9
of Ref. [3].

IV.   CONSTANT FORCE PROTOCOL

In this section we consider a filament of viscoelastic material that is initially cylindrical and undeformed, with all internal stresses well relaxed. At some time $t = 0$ it is then subject to the switch-on of a tensile force F_c, which is held constant thereafter.

For the protocol of constant imposed stress in the previous section, we showed that (to good approximation) the sample attains a state of stationary flow specified by the homogeneous extensional constitutive curve, at the given imposed stress, before starting to neck. That enabled us to consider the emergence of a necked state out of an initially homogeneous 'base state' that was stationary in time.

In important contrast, under conditions of constant force we shall find that the development of the neck happens in tandem with a continuous time evolution in the underlying homogeneous base state out of which the necked state emerges. In what follows, therefore, our strategy will be first (in Sec. IV A) to discuss the time-evolution of that homogeneous underlying base state, and then (in Sec. IV B) to discuss the way in which a neck develops as that base state evolves. As usual our analytical discussion will focus for the sake of simplicity and generality on the toy scalar constitutive model, with numerical calculations confirming the same scenario in the fully tensorial models.

A.   Base state evolution

Within the toy scalar model, the homogeneous base state obeys Eqns. II.34 to II.37. Repeating these here for convenience, we have the condition of mass balance

$$\dot{A}_0(t) = -\dot{\epsilon}_0 A_0, \qquad (IV.1)$$

while the tensile force, which is time-independent in this protocol, obeys

$$F_0 = F_c = A_0 \sigma_0 = A_0(GZ_0 + \eta\dot{\epsilon}_0), \qquad (IV.2)$$

with σ_0 the tensile stress. The viscoelastic variable obeys

$$\dot{Z}_0(t) = \dot{\epsilon}_0 f(Z_0) - \frac{1}{\tau}g(Z_0). \qquad (IV.3)$$

Immediately following the imposition of a force F_c, the stress $\sigma_0(0) = F_c/A_0(0)$, where $A_0(0)$ is the filament's initial cross sectional area. The viscoelastic contribution to the stress is initially zero, and all the load is carried by the solvent. Accordingly a uniform initial strain rate $\dot{\epsilon}_0 = F_c/A_0(0)\eta$ instantaneously establishes along the filament. This is seen in the initial values of the strain-rate signal versus time in Fig. 5b), which shows our numerical results for the base-state dynamics of the Rolie-Poly model. In the flow-curve representation of Fig. 5a), therefore, the base state's trajectory starts (for any given imposed force) on the solvent constitutive branch $\sigma_E = \eta\dot{\epsilon}$, which is shown as a dotted black line.

In contrast to the protocol of constant imposed stress, in this imposed-force protocol the stress must progressively increase in time in order to maintain a constant force as the filament stretches out and its cross sectional area thins. (Recall that the tensile force is the product of the tensile stress and the cross sectional area.) This can be seen by differentiating Eqn. IV.2 to get

$$\dot{F}_0(t) = 0 = \dot{A}_0\sigma_0 + A\dot{\sigma}_0, \qquad (IV.4)$$

which rearranges to give

$$\frac{\dot{\sigma}_0}{\sigma_0} = -\frac{\dot{A}_0}{A_0} = \dot{\epsilon}_0. \qquad (IV.5)$$

The second equality here follows from the mass balance condition IV.1. Hence, the stress increases in time with a fractional growth rate given at any time t by the strain rate $\dot{\epsilon}_0(t)$.

If the flow were to remain dominated by the Newtonian solvent, with no load transfer to the viscoelastic component, this strain rate $\dot{\epsilon}_0(t)$ would remain trivially given by $\dot{\epsilon}_0(t) = \sigma_0(t)/\eta$ for all times, and the fractional rate of stress increase would accordingly likewise equal $\sigma_0(t)/\eta$. In the flow-curve representation of Fig. 5a), the base-state's trajectory would then simply sweep up the solvent constitutive branch shown by the black dotted line. At any time t, however, there is a competing tendency of the flow to evolve away from the solvent constitutive branch to the composite constitutive curve of the combined viscoelastic and solvent components (which we hereafter call simply the viscoelastic constitutive curve), at a rate G/η. Recall Eqn. III.3 and the discussion immediately following it.

For typical initial stress values $\sigma_0 \lesssim G$, the second of these processes (of evolution to the viscoelastic constitutive curve) is faster than the first (of time-increase of the stress up the solvent branch). As a result, for these low imposed force values the system's trajectory in the flow-curve representation of Fig. 5a) quickly evolves away from the solvent constitutive branch and leftwards to the viscoelastic constitutive curve, before having chance to sweep any way up the solvent branch. This progression from the Newtonian to viscoelastic constitutive curve is associated with a fast sudden decrease in the signal of strain rate as a function of time $\dot{\epsilon}_0(t)$ at a time $t \approx 10^{-2}$ for the three lowest imposed force values in Fig. 5b). Thereafter the base state flow remains specified by the viscoelastic constitutive curve, exploring it in an upward direction as the stress increases according to Eqn. IV.5, and the strain rate likewise rapidly increasing in Fig. 5b). (In fact this discussion holds for models with a finite extensional viscosity. The Oldroyd B model exhibits different, but pathological behaviour on account of its extensional catastrophe.)

For initial stress values $\sigma_0 \gtrsim G$, in contrast, the time-increase of the stress up the solvent constitutive branch is initially faster than the evolution away from that branch. Accordingly for these larger imposed force values the
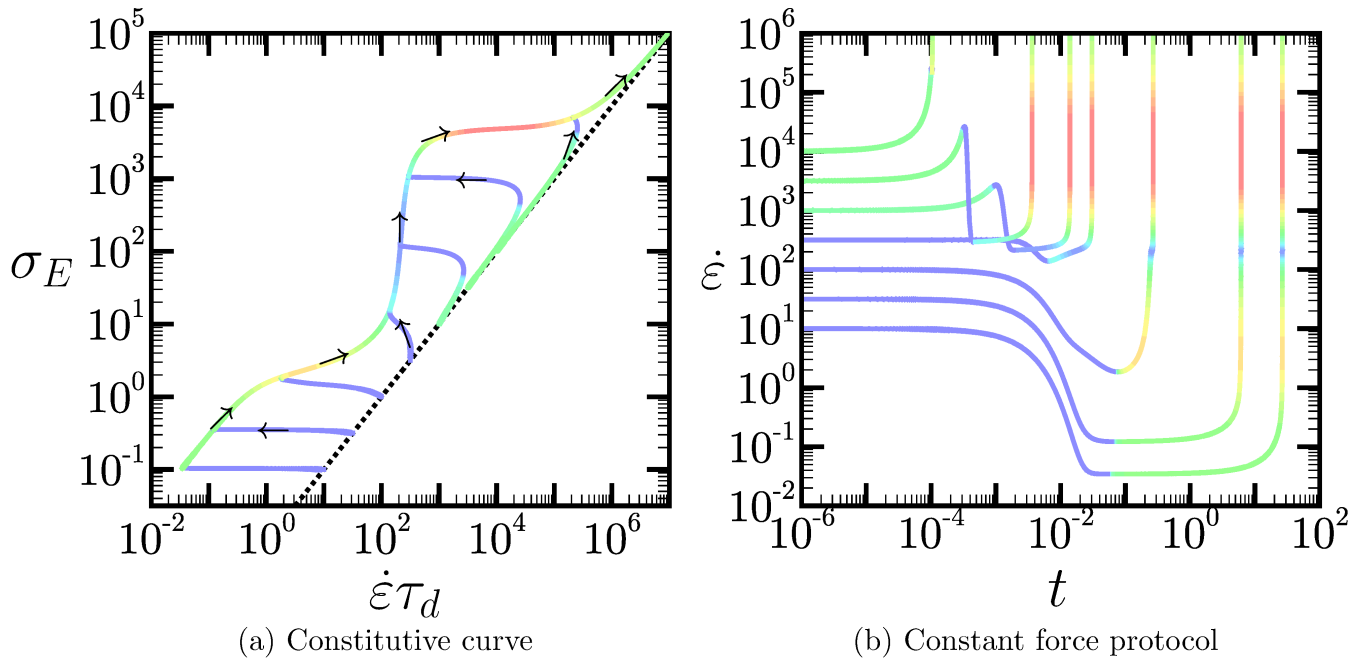
(a) Constitutive curve

(b) Constant force protocol

FIG. 5. **Finite-stretch Rolie-Poly model.** (a) Viscoelastic constitutive curve (leftmost limiting curve line) and solvent constitutive curve (dotted line). The trajectory of the base state flow is also shown, for several different imposed forces, in this flow-curve representation of stress as a function of strain rate (b) Evolution of the strain-rate with time. Imposed constant forces are $10^{n/2}$ with $n = -2 \cdots 4$ and the colourscale is the same as in figure 2 showing the value of $[d \log \sigma_{\mathrm{E}}/d \log \dot{\epsilon}]^{-1}$.

base state trajectory in the flow-curve representation of Fig. 5a) first explores the solvent constitutive curve in an upward direction, and only later makes its transit leftwards to the viscoelastic constitutive curve, with the associated sudden decrease in strain rate. Once the viscoelastic constitutive curve has been attained, the flow again explores it with increasing stress and strain rate according to Eqn. IV.5.

In any such regime where the base state flow sweeps up one of these underlying constitutive branches (whether initially that of the solvent or finally the full viscoelastic constitutive curve), the time rate of change of the stress is given by

$$\dot{\sigma}_0 = \sigma_0'(\dot{\epsilon}_0) \frac{d\dot{\epsilon}_0}{dt}, \qquad (\text{IV.6})$$

where the function $\sigma_0(\dot{\epsilon}_0)$ specifies the constitutive curve in question, and $\sigma_0'(\dot{\epsilon}_0)$ its slope. Substituting this into Eqn. IV.5, and rearranging, gives an expression for the time rate of change of the strain rate:

$$\frac{1}{\dot{\epsilon}_0} \frac{d\dot{\epsilon}_0}{dt} = \frac{\sigma_0}{\sigma_0'(\dot{\epsilon}_0)}. \qquad (\text{IV.7})$$

In any regime where the constitutive curve in question is approximately Newtonian, $\sigma_0 \propto \dot{\epsilon}_0$, this can easily be shown to lead to a blow-up of the strain rate in a finite time set by the inverse initial strain rate:

$$\dot{\epsilon}_0(t) = \frac{\dot{\epsilon}_0(0)}{1 - \dot{\epsilon}_0(0)t}. \qquad (\text{IV.8})$$

This is indeed evident in the signals of strain rate as a function of time in Fig. 5b).

Although the blow-up happens quickly in terms of time, however, the filament nonetheless develops large strains during this blow-up. In what follows, indeed, our primary focus will be on elucidating the rate at which a neck develops as a function of the accumulating strain (while also recognising that the corresponding rate of necking as a function of elapsed time will in many cases be very quick indeed).

B. Rate of necking

So far, we have discussed how a base state of homogeneous flow evolves in time under conditions of constant imposed force. In this section, we consider how a necked state develops out of that initially homogeneous time-evolving base state flow. At the level of linearised dynamics the heterogeneous perturbations $\delta\dot{\epsilon}_q(t), \delta a_q(t), \delta Z_q(t)$ that are the precursor of any neck evolve according to Eqns. II.44 to II.47, which we repeat here for convenience. The linearised mass balance condition gives

$$\partial_t \delta a_q = -\delta\dot{\epsilon}_q. \qquad (\text{IV.9})$$

The linearised force balance condition gives

$$0 = \sigma_{\mathrm{E}}\delta a_q + G\delta Z_q + \eta\delta\dot{\epsilon}_q, \qquad (\text{IV.10})$$

and the linearised viscoelastic dynamics give

$$\partial_t \delta Z_q = \delta \dot{\epsilon}_q f(Z_0) + C \delta Z_q, \qquad (IV.11)$$

in which

$$C = \dot{\epsilon} f'(Z_0) - \frac{1}{\tau} g'(Z_0). \qquad (IV.12)$$

Our aim in what follows is to relate the dynamics of these necking perturbations $(\delta \dot{\epsilon}_q(t), \delta a_q(t), \delta Z_q(t))$ to the time-evolution of the underlying base state $\dot{\epsilon}_0(t), A_0(t), Z_0(t)$. Doing so will allow us to make predictions for the rate at which a necked state develops, in terms of characteristic signatures in the rheological signals of the base state. It is also important to note that, before any significant necking occurs, the rheological signals of the base state match the bulk rheological signals measured experimentally. Therefore, our predictions for the onset of a necked state are indeed made in terms of characteristic signatures in the experimentally measured rheological quantities.

The time-evolution of the base state is specified by Eqns. IV.1 to IV.3. Differentiating these with respect to time (with the mass balance condition first pre-divided by $A_0(t)$) gives

$$\frac{d}{dt}\left(\frac{\dot{A}_0}{A_0}\right) = -\frac{d\dot{\epsilon}_0}{dt}, \qquad (IV.13)$$

$$\frac{dF_0}{dt} = 0 = \sigma_0 \frac{dA_0}{dt} + A_0 \left(G\frac{dZ_0}{dt} + \eta\frac{d\dot{\epsilon}_0}{dt}\right), \qquad (IV.14)$$

$$\frac{d\dot{Z}_0}{dt} = \frac{d\dot{\epsilon}_0}{dt} f(Z_0) + C\frac{dZ_0}{dt}. \qquad (IV.15)$$

Comparing Eqns. IV.9, IV.10 and IV.11 with Eqns. IV.13, IV.14 and IV.15, we note that the heterogeneous perturbations $(\delta \dot{\epsilon}_q(t), \delta a_q(t), \delta Z_q(t))$ to the homogeneous base state obey the same dynamical equations as the base state quantities $(\ddot{\epsilon}_0, \dot{A}_0/A_0, \dot{Z}_0)$. Therefore [52], this means that

$$\frac{1}{\delta a_q}\frac{d\delta a_q}{dt} = \frac{d}{dt}\left(\frac{\dot{A}_0}{A_0}\right)/\frac{\dot{A}_0}{A_0} = \frac{1}{\dot{\epsilon}_0}\frac{d\dot{\epsilon}_0}{dt}, \qquad (IV.16)$$

in which the final equality follow from the mass balance condition IV.1. This is an important result: it predicts that any initially small heterogeneous perturbations along the filament's length will grow towards a necked state in any regime where the bulk strain rate signal $\dot{\epsilon}_0(t)$ – *i.e.*, the time-differential of the creep curve – increases in time. A converse tendency to return towards heterogeneous flow is predicted in any regime where the strain rate decreases in time.

Looking back at Fig. 5, we recall that the strain rate indeed increases in time in any regime where the sample

sweeps up any branch of a (positively sloping) constitutive curve. The associated rate of necking per unit strain can be calculated by substituting Eqn. IV.7 for the rate of change of strain rate into Eqn. IV.16 to get

$$\frac{1}{\dot{\epsilon}_0}\frac{1}{\delta a_q}\frac{d\delta a_q}{dt} = \frac{1}{\dot{\epsilon}_0^2}\frac{d\dot{\epsilon}_0}{dt} = \frac{\sigma_0}{\dot{\epsilon}_0}\frac{d\dot{\epsilon}_0}{d\sigma_0} = \left(\frac{d\log\sigma_0}{d\log\dot{\epsilon}_0}\right)^{-1} \qquad (IV.17)$$

At any instant during the evolution of the (base state) flow up one of the underlying constitutive branches, therefore, the rate of necking per unit strain is given by the inverse slope of that constitutive curve on a log-log plot. Indeed this mirrors the result of Eqn. III.9 for the rate of necking (per unit strain) under conditions of constant imposed stress. The important difference in this case of constant imposed force is that the base state doesn't remain at a fixed point on the constitutive curve, but rather moves upward along that curve as the filament's area thins and the stress accordingly increases to maintain constant force.

In motivating the result in Eqn. IV.17, we implicitly assumed (via our use of Eqn. IV.7) that the flow state is instantaneously prescribed by the underlying constitutive curve at any value of the upwardly evolving stress. While this is true to good approximation, the flow in fact must obey the dynamical viscoelastic constitutive equation. In making that assumption, therefore, we effectively neglected one mode of the system's dynamics. Correctly accounting for the viscoelastic constitutive dynamics gives another mode of necking instability, the rate of which is set by the inverse of the same quantity $\partial_\epsilon F_{\text{elastic}}$ as in Eqn. III.8 above: we identify this as the manifestation of the elastic Considère mode in the constant force protocol.

C. Numerical results

With the predictions of the previous section in mind, we now present our linear stability results for necking in the constant force protocol. These are shown in Fig. 6, each panel (a)-(f) of which corresponds to a counterpart constitutive curve panel in Fig. 2. The data are presented in the plane $(\bar{\epsilon}, F_c)$ of accumulated strain and imposed force, which should be interpreted as follows. Any vertical cut up this plane corresponds to single experiment in which the imposed tensile force F_c is held fixed and the accumulated strain $\bar{\epsilon}$ increases up the plane as the filament stretches out under the influence of this load.

The orange and magenta dashed lines in Fig. 6 reflect our discussion of the trajectory of the base state flow in Fig. 5a) above. In particular, at any imposed force F_c the orange dashed line shows the strain at which the base state flow first departs by more than 1% from the solvent constitutive branch. The magenta dashed line shows the strain at which it attains the stationary underlying viscoelastic constitutive curve, to within 1%. (These lines merge towards the right hand side of the figure for the
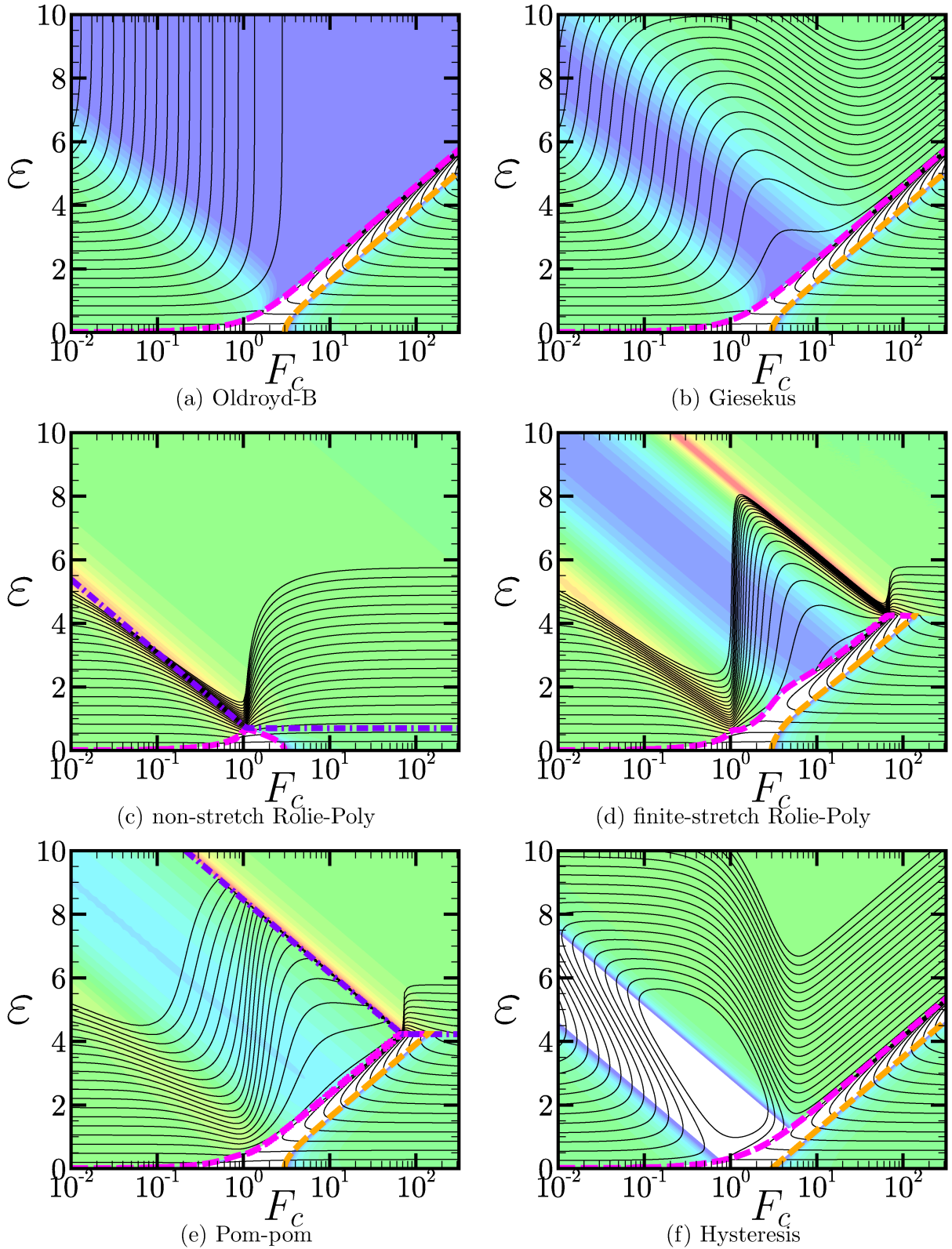
FIG. 6. **Numerical results for the linearised necking dynamics at constant imposed tensile force within the six constitutive models. In each panel the thin black lines show contours of constant area perturbations** $\delta a/\delta a_0 = 10^{n/8}$, **with** $n = 1 \cdots 20$ **in curves from bottom to top, representing the growing degree of necking at increasing strain** ϵ **upwards in any filament stretching experiment at fixed imposed force** F_c**. The orange dashed line shows the strain at which the underlying base state first departs the solvent constitutive branch by more than** 1%**. The magenta dashed lines show the strain at which the underlying base state attains the underlying homogeneous viscoelastic constitutive curve, to within** 1%**. The purple dot-dashed line shows the strain at which the elastic Considère mode becomes unstable. The colours show the rate of necking for any** $(\bar{\epsilon}, F_c)$**, using the same colourscale as in figure** **2**. **Regions of stability against necking are shown in white.**

finite-stretch Rolie-Poly and Pom-pom models: at very high stresses in these models the constitutive curve is dominated by the solvent contribution.)

The solid black lines show contours of constant area perturbation $\delta a(t)$. Each successive contour corresponds to an increase in the degree of necking $\delta a(t)$ by a factor $10^{1/8}$. The nth contour thus represents a degree of necking $\delta a / \delta a_0 = 10^{n/8}$, where δa_0 is the small initial seeding at the start of the run. The more densely clustered the contour lines vertically at any fixed F_c, therefore, the faster necking occurs in an experiment at that imposed force.

Focusing first for definiteness on our results for the Giesekus model in panel b), we see that for any imposed force $F_c \lesssim 1.0$ the base state flow quickly transits to the viscoelastic constitutive curve as the strain increases vertically up the panel at that fixed F_c, without first exploring the Newtonian branch. Indeed, the scale of strain over which this transit happens is barely discernible. After attaining the viscoelastic constitutive curve the flow progressively sweeps up it as the filament stretches out with accumulating strain $\bar{\epsilon}(t)$, thins in area as $\exp(-\bar{\epsilon}(t))$, and the stress correspondingly increases to maintain a constant force. At any accumulated strain $\bar{\epsilon}$, for the given imposed F_c, the colourscale in Fig. 6b) shows the inverse logarithmic slope of the constitutive curve at the stress that has been attained by that strain, matching the colourscale in Fig. 2b). Recall from Eqn. IV.17 that this sets the rate at which the neck will be developing at any time t, or correspondingly accumulated strain $\bar{\epsilon}(t)$, during the stretching process. For example, for a representative imposed force $F_c = 0.1$ in Fig. 6b), the flow quickly attains the viscoelastic constitutive curve of Fig. 2b) at a stress $\sigma_E \approx 0.1$. It then transits up the slow-flow Newtonian part of of this viscoelastic constitutive curve, with an $O(1)$ rate of necking indicated in green, then transits the steeply sloping part it, with a slower rate of necking indicated in blue, then finally transients the Newtonian fast-flow part of it, with a return to the $O(1)$ rate of necking indicated in green.

In contrast, for a representative imposed force $F_c = 100.0$ in Fig. 6b), the base state flow initially evolves up the solvent constitutive branch $\sigma_E = \eta\dot{\epsilon}$ (not shown in Fig. 2b), with an $O(1)$ rate of necking indicated in green. Between a strain of roughly 4 and 5 it then makes a rapid transit to the Newtonian fast-flow part of the viscoelastic constitutive curve in Fig. 2b), during which the degree of necking actually decays slightly. Finally, it transients up that fast-flow part of the viscoelastic constitutive curve, again with an $O(1)$ rate of necking indicated in green.

Although we have focused the discussion here on the Giesekus model for the sake of a definite example, a closely analogous explanation underpins essentially all the results in Fig. 6. To summarise: under conditions of a constant imposed force the flow typically sweeps up the underlying viscoelastic constitutive curve of the material. At any given time, the rate of necking is given by the inverse of the slope of that constitutive curve, shown in a log-log plot, at the stress that has been attained by that time. For low imposed forces the flow first sweeps up the constitutive curve of the solvent contribution, before transiting to the viscoelastic curve.

One further feature appears in the results for the non-stretch Rolie-Pole and Pom-Pom models in Figs. 6c) and e) respectively: here the elastic Considère mode also operates, and is marked as a purple dot-dashed line on the figures.

V. CONCLUSIONS

By means of linear stability analysis and nonlinear simulations performed at the level of a slender filament approximation, we have studied the onset of necking during the stretching of an initially cylindrical filament of complex fluid or soft solid, separately under conditions of constant imposed tensile stress and constant imposed tensile force. Our results pertain to highly viscoelastic filaments of large enough radius that bulk stresses dominate surface effects, with surface tension neglected accordingly.

Under conditions of constant imposed tensile stress, the flow first quickly attains a state with the strain rate prescribed by the underlying homogeneous stationary extensional constitutive curve of the fluid in question, at the given imposed stress value. During this early time regime, the filament remains homogeneous to good approximation, without any significant necking. A second regime then ensues in which that initially homogeneous flow destabilises to the formation of a neck. This instability can occur via one of two modes, the first of which arises widely across all the constitutive models that we have studied, while the second is rarer in comparison.

The first mode of instability has a characteristic rate of necking per accumulated Hencky strain unit set by the inverse of the slope of the underlying stationary homogeneous constitutive curve, on a log-log plot, at the given imposed stress. This is an important result: essentially all materials of which we are aware have a positively sloping extensional constitutive curve, and should therefore be unstable to necking under conditions of a constant imposed tensile stress. This prediction is indeed consistent with ubiquitous reports of necking in the literature.

A possible rare exception to this "constitutive curve" mode of necking is however predicted in a material that has a non-monotonic extensional constitutive curve, for imposed stresses in the regime where that curve has negative slope, such as could arise in polymer solutions displaying coil-stretch hysteresis [34–36]. It would be interesting to study the implications of the analysis offered here in that case. It would also be interesting to consider the implications of the presence of a yield stress in a material for necking (or its possible absence) at imposed stresses below yield, where the constitutive curve is essentially vertical. Necking in constant strain rate and constant velocity protocols in a yield stress fluid were discussed previously in [53].

Under these conditions of a constant imposed stress a second, more dramatic mode of necking instability can also arise. This is essentially the direct counterpart of the elastic Considère mode predicted earlier by ourselves in the context of filament stretching at constant imposed Hencky strain rate [18]. However it arises relatively rarely: of the six constitutive models studied in this work, it only occurs in only two of them, and in a relatively restricted regime of strain rate in each case. In particular, it arises in models of polymeric flow in which polymer chain stretch is dramatically inhibited: in the Rolie-Poly model of linear entangled polymers with chain stretch disallowed, and in the Pom-Pom model of branched entangled polymers with a hard cutoff in the permitted degree of chain stretch.

We have also studied the onset of necking under conditions of constant imposed tensile force. In this protocol, in contrast to the case of constant tensile stress, the stress progressively increases over time in order to maintain a constant tensile force as the filament stretches out and gets thinner. (Recall that the force is the product of the stress and the filament's cross sectional area.) Typically, the flow simply sweeps progressively up one of the fluid's underlying constitutive branches (whether that of the solvent, or the full viscoelastic constitutive curve). At any time during this progression the rate of necking is set by the inverse of the slope of that constitutive curve (on a log-log plot), at the stress that has been attained by that time, in close analogy with the case of a constant imposed stress. Accordingly, a neck is predicted to develop in any regime in which the measured strain rate signal increases in time. During progression up a Newtonian or quasi-Newtonian part of a constitutive curve, a finite-time divergence is predicted in the signal of strain rate (and associated rate of necking) as a function of time. The elastic Considère mode also operates in the non-stretch Rolie-Poly and Pom-Pom models in some regimes.

Throughout this manuscript we have restricted ourselves to regimes relevant to our slender filament approximation, in which the wavelength of any heterogeneities that develop along the length of the filament are long compared with the filament radius. The manner in which these 'fluid-like' necking instabilities cross over to more dramatic solid-like fracturing at very high imposed loads, where the sample sharply rips across its cross section, remains an interesting open issue.

* d.m.hoyle@durham.ac.uk; http://community.dur.ac.uk/d.m.hoyle/

† suzanne.fielding@durham.ac.uk;
http://community.dur.ac.uk/suzanne.fielding/

[1] G. H McKinley and T Sridhar. Filament-Stretching Rheometry of Complex Fluids. *Annual Review of Fluid Mechanics*, 34(1):375–415, 2002.

[2] H Münstedt. Viscoelasticity of polystyrene melts in tensile creep experiments. *Rheologica Acta*, 14:1077–1088, 1975.

[3] H Münstedt and Z Starý. Steady states in extensional flow of strain hardening polymer melts and the uncertainties of their determination. *Journal of Rheology*, 57 (4):1065, 2013.

[4] H Münstedt. Rheological experiments at constant stress as efficient method to characterize polymeric materials. *Journal of Rheology*, 58(3):565–587, 2014.

[5] S Kurzbeck, F Oster, H Munstedt, T. Q Nguyen, and R Gensler. Rheological properties of two polypropylenes with different molecular structure. *Journal of Rheology*, 43(2):359, 1999.

[6] H. M Laun and H Münstedt. Comparison of the elongational behaviour of a polyethylene melt at constant stress and constant strain rate. *Rheologica Acta*, 15(October): 517–524, 1976.

[7] H. M Laun and H Münstedt. Elongational behaviour of a low density polyethylene melt - I. Strain rate and stress dependence of viscosity and recoverable strain in the steady-state. Comparison with shear data. Influence of interfacial tension. *Rheologica Acta*, 17:415–425, 1978.

[8] H Münstedt and D. W Auhl. Rheological measuring techniques and their relevance for the molecular characterization of polymers. *Journal of Non-Newtonian Fluid Mechanics*, 128(1):62–69, jun 2005.

[9] H Münstedt and H. M Laun. Elongational behaviour of a low density polyethylene melt - II. Transient behaviour in constant stretching rate and tensile creep experiments. Comparison with shear data. Temperature dependence of the elongational properties. *Rheologica Acta*, 18:492–504, 1979.

[10] F Wolff, J. A Resch, J Kaschta, and H Münstedt. Prediction of steady-state viscous and elastic properties of polyolefin melts in shear and elongation. *Rheologica Acta*, 50(7-8):645–653, 2011.

[11] N. J Alvarez, J Marín, Q Huang, M Michelsen, and O Hassager. Creep Measurements Confirm Steady Flow after Stress Maximum in Extension of Branched Polymer Melts. *Physical Review Letters*, 110(16):168301, apr 2013.

[12] M. H Wagner, H Bastian, A Bernnat, S Kurzbeck, and C. K Chai. Determination of elongational viscosity of polymer melts by RME and Rheotens experiments. *Rheologica Acta*, 41(4):316–325, may 2002.

[13] P Szabo, G. H McKinley, and C Clasen. Constant force extensional rheometry of polymer solutions. *Journal of Non-Newtonian Fluid Mechanics*, 169-170:26–41, feb 2012.

[14] J Matta and R Tytus. Liquid stretching using a falling cylinder. *Journal of Non-Newtonian Fluid Mechanics*, 35 (2-3):215–229, jan 1990.

[15] T Raible and S Stephenson. Constant Force Elongational Flow of a low-density polyethylene melt - Experiment

and Theory. *Journal of Non-Newtonian ...*, 11:239–256, 1982.

[16] M. H Wagner and V. H Rolon-Garrido. Constant force elongational flow of polymer melts: Experiment and modelling, 2012.

[17] S. M Fielding. Criterion for Extensional Necking Instability in Polymeric Fluids. *Physical Review Letters*, 107 (25):258301, dec 2011.

[18] D. M Hoyle and S. M Fielding. Criteria for extensional necking instability in complex fluids and soft solids. Part I: imposed Hencky strain rate protocols. *Journal of Rheology*, 60:XXX–XXX, 2016.

[19] V. C Barroso and J. M Maia. Influence of long-chain branching on the rheological behavior of polyethylene in shear and extensional flow. *Polymer Engineering & Science*, 45(7):984–997, jul 2005.

[20] G Liu, H Ma, H Lee, H Xu, S Cheng, H Sun, T Chang, R. P Quirk, and S.-Q Wang. Long-chain branched polymers to prolong homogeneous stretching and to resist melt breakup. *Polymer*, 54(24):6608–6616, 2013.

[21] T. I Burghelea, Z Starý, and H Münstedt. On the viscosity overshoot during the uniaxial extension of a low density polyethylene. *Journal of Non-Newtonian Fluid Mechanics*, 166(19-20):1198–1209, oct 2011.

[22] A Tripathi, K. C Tam, and G. H McKinley. Rheology and Dynamics of Associate Polymer Solutions in Shear and Extension: Theory and Experiments. *Macromolecules*, 39:1981–1999, 2006.

[23] A Bhardwaj, E Miller, and J. P Rothstein. Filament stretching and capillary breakup extensional rheometry measurements of viscoelastic wormlike micelle solutions. *Journal of Rheology*, 51(2007):693, 2007.

[24] M Arciniaga, C.-C Kuo, and M Dennin. Size dependent brittle to ductile transition in bubble rafts. *Colloids and Surfaces A: Physicochemical and engineering aspects*, 382 (1-3):36–41, jun 2011.

[25] M. I Smith, R Besseling, M. E Cates, and V Bertola. Dilatancy in the flow and fracture of stretched colloidal suspensions. *Nature communications*, 1(8):114, jan 2010.

[26] R. J Andrade and J. M Maia. A study on the flow, failure, and rupture mechanisms of low-density polyethylene in controlled-stress uniaxial extensional flow. *Journal of Rheology*, 55(5):925–937, 2011.

[27] A. Y Malkin, A Arinstein, and V. G Kulichikhin. Polymer extension flows and instabilities. *Progress in Polymer Science*, 39(5):959–978, 2014.

[28] Y Wang, P Boukany, S.-Q Wang, and X Wang. Elastic breakup in uniaxial extension of entangled polymer melts. *Physical Review Letters*, 99(December):1–4, 2007.

[29] M Considère. Memoire sur l'emploi du fer et de l'acier dans les constructions. *Ann. Ponts Chaussees*, 9:574, 1885.

[30] R. G Larson. *Constitutive equations for polymer melts and solutions*. Butterworth Publishers, Stoneham, 1988.

[31] A. E Likhtman and R. S Graham. Simple constitutive equation for linear polymer melts derived from molecular theory: RoliePoly equation. *Journal of Non-Newtonian Fluid Mechanics*, 114(1):1–12, sep 2003.

[32] R. J Blackwell, T. C. B McLeish, and O. G Harlen. Molecular dragstrain coupling in branched polymer melts. *Journal of Rheology*, 44(1):121, 2000.

[33] T. C. B McLeish and R. G Larson. Molecular constitutive equations for a class of branched polymers: The pom-pom polymer. *Journal of Rheology*, 42(February):

81, 1998.

[34] S Somani, E. S. G Shaqfeh, and J. R Prakash. Effect of Solvent Quality on the CoilStretch Transition. *Macromolecules*, 43(24):10679–10691, dec 2010.

[35] C. M Schroeder. Observation of Polymer Conformation Hysteresis in Extensional Flow. *Science*, 301(5639):1515–1519, sep 2003.

[36] P. G De Gennes. Coil-stretch transition of dilute flexible polymers under ultrahigh velocity gradients. *The Journal of Chemical Physics*, 60(12):5030, 1974.

[37] C Clasen, J Eggers, M. a Fontelos, J Li, and G. H McKinley. The beads-on-string structure of viscoelastic threads. *Journal of Fluid Mechanics*, 556:283, may 2006.

[38] M Tembely, D. C Vadillo, M. R Mackley, and A Soucemarianadin. The matching of a one-dimensional numerical simulation and experiment results for low viscosity Newtonian and non-Newtonian fluids during fast filament stretching and subsequent break-up. *Journal of Rheology*, 56(1):159–183, 2012.

[39] D. C Vadillo, M Tembely, N. F Morrison, O. G Harlen, M. R Mackley, and A Soucemarianadin. The matching of polymer solution fast filament stretching, relaxation, and break up experimental results with 1D and 2D numerical viscoelastic simulation. *Journal of Rheology*, 56(6):1491–1516, 2012.

[40] M. F Webster, H Matallah, K Sujatha, and M. J Banaai. Numerical modelling of step-strain for stretched filaments. *Journal of Non-Newtonian Fluid Mechanics*, 151:38–58, 2008.

[41] C McIlroy and O. G Harlen. Modelling capillary breakup of particulate suspensions. *Physics of Fluids*, 26(3): 033101, mar 2014.

[42] P. P Bhat, O. a Basaran, and M Pasquali. Dynamics of viscoelastic liquid filaments: Low capillary number flows. *Journal of Non-Newtonian Fluid Mechanics*, 150: 211–225, 2008.

[43] M Doi and S Edwards. *The Theory of Polymer Dynamics*. Oxford University Press, Oxford, 1986.

[44] G Marrucci. Dynamics of entanglements: A nonlinear model consistent with the Cox-Merz rule. *Journal of Non-Newtonian Fluid Mechanics*, 62(2-3):279–289, 1996.

[45] G Ianniruberto and G Marrucci. Convective constraint release (CCR) revisited. *Journal of Rheology*, 58(1):89, 2014.

[46] G Ianniruberto and G Marrucci. Do Repeated Shear Startup Runs of Polymeric Liquids Reveal Structural Changes? *ACS Macro Letters*, 3(6):552–555, jun 2014.

[47] M. E Cates. Nonlinear viscoelasticity of wormlike micelles (and other reversibly breakable polymers). *The Journal of Physical Chemistry*, 94(1):371–375, jan 1990.

[48] M. G Forest and Q Wang. Change-of-type behavior in viscoelastic slender jet models. *Theoretical and Computational Fluid Dynamics*, 2(1):1–25, 1990.

[49] D. O Olagunju. A 1-D theory for extensional deformation of a viscoelastic filament under exponential stretching. *Journal of Non-Newtonian Fluid Mechanics*, 87:27–46, 1999.

[50] M. M Denn, C. J. S Petrie, and P Avenas. Mechanics of steady spinning of a viscoelastic liquid. *AIChE Journal*, 21(4):791–799, 1975.

[51] W. H Press, S. A Teukolsky, W. T Vetterling, and B. P Flannery. *Numerical Recipes 3rd Edition: The art of Scientific Computing*. Cambridge University Press, New York, 2007.

[52] Note1. Technically, the equality IV.16 only holds if the initial conditions of $(\delta\dot{\epsilon}_q(t), \delta a_q(t), \delta Z_q(t))$ are the same as those for $(\ddot{\epsilon}_0, \dot{A}_0/A_0, \dot{Z}_0)$. This will not in general be the case. However, after an initial transient associated with any discrepancy in the initial conditions, we find that Eqn. IV.16 indeed holds well in all the constitutive models that we have studied.

[53] D. M Hoyle and S. M Fielding. Age-Dependent Modes of Extensional Necking Instability in Soft Glassy Materials. *Physical Review Letters*, 114(15):158301, 2015.